Formation of primordial black holes in the early universe

A project report
submitted in partial fulfillment for the award of the degree of
Master of Science
in
Physics
by

Saurav Mishra

under the guidance of
Prof. L. Sriramkumar

Department of Physics
Indian Institute of Technology Madras
Chennai 600036, India

May 2022

CERTIFICATE

This is to certify that the project titled **Formation of primordial black holes in the early universe** is a bona fide record of work done by **Saurav Mishra** towards the partial fulfillment of the requirements of the Master of Science degree in Physics at the Indian Institute of Technology, Madras, Chennai 600036, India.

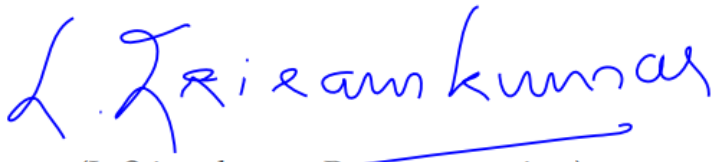

(L. Sriramkumar, Project supervisor)

ACKNOWLEDGEMENTS

Foremost, I would like to express my sincere gratitude to my project supervisor Prof. L. Sriramkumar for his valuable guidance and supervision throughout the project. I am also grateful for his patience, motivation, enthusiasm, and immense knowledge during the tough time of the COVID-19 pandemic where most of the work was done virtually. Apart from that, I would also thank him for supporting and advising me continuously.

I am also thankful to Dr. Sanil Unnikrishnan for his precious discussions and continuous support. I would also like to thank Tamal Mukherjee, Suvashis Maity, Sagarika Tripathy, Rahul Priyadarshan, and Satvik Mishra for important discussions and support. I also thank my family for being the support system throughout difficult times.

A big thanks to my friends Anmol, Anubhav, Neelkanth, Siddharth, Neelam, Shallika, Shruti, Rohit, Aadrit, and Jaspreet for the mental and emotional support they rendered throughout the tough times of the pandemic.

ABSTRACT

Recent observations of the gravitational waves (GWs) from the merged binary black holes have sparked an interest in whether such black holes have a primordial origin or not. Another interest has been to study primordial black holes as a cold dark matter candidate. This project is aimed to study the generation of primordial black holes (PBHs) through the inflation scenario and their contribution to the cold dark matter. In this report, we have studied two scenarios: ultra-slow inflation and punctuated inflation. We have outlined the formation of such black holes through the collapse of large density fluctuations that were generated during inflation during radiation domination. We found that it is possible to produce a copious amount of primordial black holes by enhancing the power spectrum on small scales when comparing the power spectrum with large scales (CMB scales) which is well constrained by the recent Planck data. It has been found that (based on the parameters of the different potentials) PBH of mass $10^{-16}\, M_{\odot}$ can account for 1.5 % of the dark matter at present.

Contents

Chapter 1

Introduction

Primordial Black Holes (PBHs) are light black holes that can be formed in the early universe. Though several formation mechanisms exist in the literature such as cosmic string loops [1], bubble formation [2], grand unified theories [3], tachyonic reheating [4], phase transitions [5], and the large density perturbation's collapse [6]. But in this report, we will mainly focus on the collapse of large density perturbation generated by the inflation during radiation domination. The study of the formation of PBHs originates back half a century ago. PBHs were realized early as a strong candidate for dark matter because it is not an elementary particle and is naturally long-lived.

1.1 A bit of history

Y. Zel'dovich, I. Novikov [7], and S. Hawking [8] discussed the PBHs for the first time. During his studies on PBHs, Hawking discovered the famous Black holes (BHs) evaporation. It was the work of B. Carr [9] and G. Chapline [10] that related PBHs contribution to the dark matter in our cosmos. Today only PBH of mass greater than 10^{15} g exists today due to the Hawking evaporation and they contribute to the cold dark matter. PBH dark matter behaves like particle dark matter on the cosmological scales. An interesting property of PBH as cold dark matter candidate is that in order to explain this we do not need any new particle to explain them. We need to modify the early universe description at the small scales such that it is consistent with the observed constraints on the large scales which account for

large density fluctuations. A considerable amount of work was done to constrain the PBHs abundance by using their peculiar properties at the small scales which would eventually lead to apparent effects such as lensing, electromagnetic emission from accretion processes, gravitational waves, etc.

In the 1990s, the MACHO collaboration's 2 years [11] Large Magellanic Cloud microlensing results ignited an interest in PBHs. The result suggests if we assume PBHs exist in our Milky Way, a significant fraction of the mass in our Milky Way is composed of sub-solar compact objects. EROS [12] and OGLE [13] results outdated the claim and it suggested only a small fraction of mass could be in the form of sub-solar PBHs. This eventually constrained the PBH abundance in sub-solar mass range.
A second wave was ignited by the famous detection of gravitational waves (GWs) by the LIGO/VIRGO collaboration [14]. It was realized that the observed signal could be compatible with PBHs merger. It even did not violate the bound requiring PBHs to be at most as abundant as the dark matter in our universe.

1.2 Consequences of PBHs discovery

It is still not clear whether PBHs formed or not, if they did, they could have numerous consequences on our current understandings of the universe even if the PBHs consist of only a small portion of dark matter. The following mentioned statements are a few motivating points:

- PBHs provide a unique probe to the early universe [15] . This could provide information on small-scale physics.
- This could be a test of primordial non-Gaussianities [16].
- Mereger events produced by PBH could be detected by LIGO/VIRGO collaboration even though it accounts for a small fraction of cold dark matter [17].
- They could be the primordial seeds for the supermassive BHs formation [18] (observed at high redshift).

- They can help in constraining the physics related to PBHs even if they never existed.

1.3 Outline of the report

The report is organized in the following way. In chapter 2, we discuss the need for inflation. We begin with the preliminaries of cosmology and the motivation for inflation. In chapter 3, we focus on the inflation and background evolution of certain models and compare the analytical and numerical results. In chapter 4, we introduce one of the famous features of inflation, i.e., perturbations and power spectrum, and would discuss in detail, certain models. In chapter 5, we describe the numerical approach to generating power spectrum and compare the available analytical solutions for the power spectra of models mentioned in the literature. In chapter 6, we discuss PBH formation and its contribution to cold dark matter. In the end, we conclude the report with the observed constraints on the PBHs.

1.4 Notation and units

We use the metric with signature (+ - - -). Greek indices (μ, ν, ...) going from 0 to 3 denote space-time coordinates whereas Latin indices (i,j,..) goes from 1 to 3 (spatial coordinates). We work in the natural units c=h=k_B=1 and defined the Planck mass $M_{\rm Pl}$=$1/\sqrt{8\pi G}$

Chapter 2

Why do we need inflation?

The hot big bang model has emerged to be the best available model related to the origin of our universe. A cataclysmic event, called the big bang, happened some 10^{10} years ago, when the universe came into existence and expanded away from a singular point. At the earliest phases, our universes consisted of radiation at incredibly high temperatures and densities. As the expansion was in the act, density and temperature fell and electrons, protons, and neutrons emerged from the radiation bath. Further, heavier elements were born from simple atoms such as hydrogen, and helium. Apparently, during this phase, this model prediction has been consistent with observations. The development of the hot big bang model has made use of our understanding of local physical laws and it has proved extremely successful, to date, in providing insight into the structure of the universe.

2.1 Friedmann line element

Survey of 2DF (2-Dimensional Field) [19], SDSS (Sloan Digital Sky Survey) [20], and DES (Dark Energy Survey) [21] suggest that universe at the scale of 100 Mpc or more is homogeneous and isotropic. The general metric which captures the homogeneity and isotropy of the universe, can be written by multiplying the space part with a time dependent term $a(t)$

$$ds^2 = dt^2 - a^2(t)\left(\frac{dr^2}{1-Kr^2} + r^2 d\theta^2 + r^2 sin^2\theta d\phi^2\right) \tag{2.1}$$

Through conformal transformation $d\eta = dt/a(t)$, metric (2.1) reduces to

$$ds^2 = a^2(\eta)\left(d\eta^2 - \frac{dr^2}{1-Kr^2} - r^2 d\theta^2 - r^2 sin^2\theta d\phi^2\right) \tag{2.2}$$

where spatial part is written in term of spherical polar co-ordinates r, θ, and ϕ. The constant K with K = 0, $\pm$1 corresponds to flat, close and open universe. The geometry exhibits by above line element know as a Friedmann-Robsertson-Walker spacetime. Upon using, Einstein field equation

$$G^\mu_\nu = R^\mu_\nu - \frac{\delta^\mu_\nu}{2}R = \frac{8\pi G}{c^4}T^\mu_\nu \tag{2.3}$$

where G^μ_ν = is Einstein Tensor. T^μ_ν is stress- energy tensor, defined as

$$T^\mu_\nu = (\rho + p)u^\mu u_\nu - p\delta^\mu_\nu \tag{2.4.a}$$

$$T^\mu_\nu = \begin{pmatrix} \rho(t) & & & \\ & -p(t) & & \\ & & -p(t) & \\ & & & -p(t) \end{pmatrix} \tag{2.4.b}$$

where ρ and p are the energy density and the pressure density of the perfect fluid respectively.

2.2 Friedmann equations

On solving Einstein equation for FLRW universe, one obtains

$$\left(\frac{\dot{a}}{a}\right)^2 + \frac{K}{a^2} = \frac{8\pi G}{3}\rho \tag{2.5.a}$$

$$\frac{\ddot{a}}{a} = -\frac{4\pi G}{3}(\rho + 3p) \tag{2.5.b}$$

$$\dot{\rho} + 3\left(\frac{\dot{a}}{a}\right)(\rho + p) = 0 \tag{2.5.c}$$

These are called Friedmann equations, which are the evolution equation of a (scale factor), ρ (energy density), and p (pressure density). The Hubble parameter is defined as

$$H \equiv \frac{\dot{a}}{a} \tag{2.6}$$

2.3 Constituents of universe

In order to solve the Friedmann equations, we need to provide an additional information regarding the equation of state, such that p is function of ρ. We assume a linear relation between them

$$p = w\rho \tag{2.7}$$

where w is state parameter. Upon integrating equation (2.5.c), we get

$$\rho \propto a^{-3(1+w)} \tag{2.8}$$

Using above result and eq. (2.5.a) for K = 0 i.e., spatial flat universe, we obtain

$$a(t) \propto \begin{cases} t^{\frac{2}{3(1+w)}}, & w \neq -1, \\ e^{Ht}, & w = -1 \end{cases} \tag{2.9}$$

For different epoch, w is shown in table 2.1

	w	$\rho(a)$	$a(t)$	$a(\tau)$	τ_i
Matter Domination	0	a^{-3}	$t^{2/3}$	τ^2	0
Radiation domination	$1/3$	a^{-4}	$t^{1/2}$	τ	0
Cosmological constant - Λ	-1	a^0	e^{Ht}	-τ^{-1}	∞

Table 2.1: FLRW solutions for a universe with K = 0 at different epoch. Ref. TASI Lectures on Inflation, Daniel Baumann [22]

We define ρ_c and the density parameter Ω (both are useful in defining the ingredients of the universe as

$$\rho_c(t) = \frac{3H^2}{8\pi G}, \qquad \Omega = \frac{\rho}{\rho_c} \tag{2.10}$$

where $\rho_c(t_o)$ is $1.88h^2 \times 10^{-26} kgm^{-3}$. Hence, the Friedmann equation (2.5.a) can be modified as

$$\Omega - 1 = \frac{\rho}{3H^2/8\pi G} = \frac{K}{a^2H^2} \tag{2.11}$$

where Ω: ratio of energy density ρ to critical energy density ρ_c. ‘

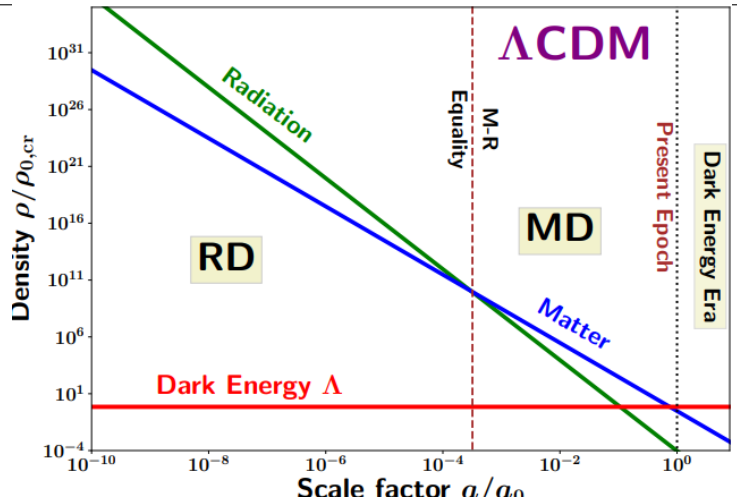

Figure 2.1: $\rho/\rho_{o,cr}$ vs a/a_o for different constituents of a flat universe. Ref. [23]

2.4 Drawbacks of the hot big bang model

Despite all its successes [24] [25], there remain some unsatisfactory aspects of the Hot Big Bang theory. The two unanswered questions which are in this model: why is the universe so close to flat today? Why is it so large, making the observed universe an 'improbable accident'. They are the motivation for need of the inflation.

2.4.1 The flatness Problem

The total energy density parameter of the universe is Ω_{tot}, which is close to the critical density. Very conservatively, it is known (from cosmic microwave background radiation (CMBR)) to lie in the range $\Omega_{tot} \leq 10^{-2}$ [24]. Geometrically, it means that the universe is quite close to the flat (Euclidean) geometry. Eq. (2.11) can be rewritten as with modulus as

$$|\Omega_{tot}(t) - 1| = \frac{|K|}{a^2(t)H^2(t)} \tag{2.12}$$

As the Ω_{tot} is nearly equal to one, we can assume a situation where we have a conventional universe (matter + radiation). We are ignoring the contribution through the cosmological constant and curvature. Using the solutions ignoring the curvature term, we find

that [24] [25]

$$|\Omega_{tot}(t) - 1| \propto \frac{1}{a^2 a^{-4}} \propto a^2 \quad \text{(radiation domination)}, \tag{2.13.a}$$

$$|\Omega_{tot}(t) - 1| \propto \frac{1}{a^2 a^{-3}} \propto a \quad \text{(matter domination)}. \tag{2.13.b}$$

In either case, $|\Omega_{tot}\text{-}1|$ is an increasing function of time. Since today , $|\Omega_o\text{-}1|$ is almost zero at present, we can determine its value at t_{Pl} (the time at which the temperature of the universe is $T_{\rm Pl} \sim 10^{19}$ Gev). As the universe's temperature varies inversely with the scale factor ($T \propto 1/a$), one can write

$$\frac{|\Omega - 1|_{T=T_{\rm Pl}}}{|\Omega - 1|_{T=T_{\rm o}}} \approx \left(\frac{a^2_{\rm Pl}}{a^2_{\rm o}}\right) \approx \left(\frac{T^2_{\rm Pl}}{T^2_{\rm o}}\right) \approx \mathcal{O}(10^{-64}) \tag{2.14}$$

where "o" stands for the present epoch, and $T_0 \sim 10^{-13}$ GeV is the present day temperature of the CMBR. To get the $(\Omega_0\text{-}1) \sim 1$ at present, $(\Omega\text{-}1)$ at early times has to be fine-tuned amazingly close to zero, but without being exactly zero. This is the famously known as flatness problem and also termed as the 'fine tuning problem'.

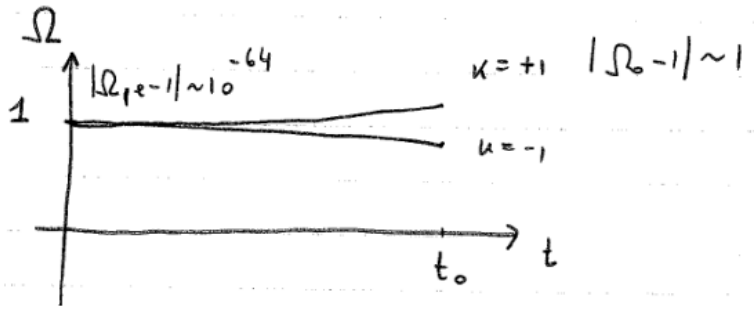

Figure 2.2: Flatness problem in the standard cosmology. Ref. [25]

2.4.2 The horizon problem

In FLRW universe(2.1), the horizon, i.e., the size of a causally connected region, is defined as the physical radial distance travelled by a light ray from the big bang singularity at t=0 upto a given time t. It is defined as [26]

$$h(t) = a(t) \int_0^t \frac{1}{a(t')} dt' \tag{2.15}$$

One can compare the size of the forward and the backward light cone at the time of decoupling by assuming that the universe was matter-dominated from t_{dec} (time of decoupling) until today t_o. One can find the physical size of the region on the last scattering surface (this is when the photons decoupled from the electrons and baryons at a red shift(z) $\sim$ 1100 and temperature$\sim$ 0.3 eV)

$$l_B(t_0, t_{dec}) = a_{dec} \int_{t_{dec}}^{t_0} \frac{1}{a(t')} dt' \simeq 3(t_{dec}^2 t_0)^{1/3} \tag{2.16}$$

where a_{dec} is scale factor at decoupling. Further assuming that from the big bang to the epoch of decoupling, universe was radiation dominated, one finds

$$l_F(0, t_{dec}) = a_{dec} \int_{0}^{t_{dec}} \frac{1}{a(t')} dt' = 2t_{dec} \tag{2.17}$$

The ratio, R is defined as ratio of the length of backward to the forward light cones at decoupling. It is equal to

$$R = \left(\frac{l_B}{l_F}\right) = \left(\frac{3}{2}\right)\left(\frac{t_0}{t_{dec}}\right)^{1/3} \simeq 70 \tag{2.18}$$

where $t_o \simeq 10^{10}$ years and $t_{dec} \simeq 10^5$ years. Though the forward light cone is almost 70 times smaller than the backward light cone, we find the cosmic microwave background radiation (CMBR) turns out to be extraordinarily isotropic. This is famously known as the horizon problem.

One can state the the horizon problem in an alternate way. Suppose λ is associated with the physical scale of perturbations for different modes and it grows as a scale factor, i.e., $\lambda \propto a$. For the power-law expansion ($a \propto t^p$), the Hubble radius[1], defined as H^{-1}, goes as a^p. For the radiation and matter epoch, p is smaller than 1. This implies that λ grows faster than the corresponding Hubble radius as we move forward in time (Fig. 2.3) [26]. This means that the primordial perturbations on the scales larger than the Hubble radius are not correlated at early times. Consequently, this fails to explain the anisotropies observed in the CMBR, and the temperature of the radiation in all directions has been the same (2.73 K).

[1]Hubble radius is a scale at which a mode will start feeling the expansion of the universe. It also defines a causal region.

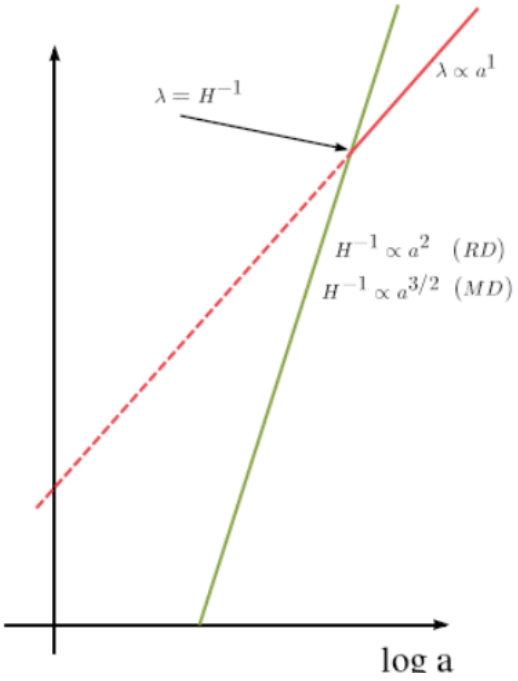

Figure 2.3: The Hubble radius (green) and a perturbation scale λ (red) vs a scale factor. Ref. [25]

Chapter 3

Inflation and background evolution

Inflation was proposed to resolve the problems with the hot big bang model. Inflation is defined as a period of evolution of the universe during which the universe expanded rapidly and the double derivative of a becomes larger than 0.

$$INFLATION \Longleftrightarrow \ddot{a} > 0 \Longleftrightarrow (\rho + 3p) < 0 \tag{3.1}$$

Perturbation of the length scales ($1 \lesssim \lambda_0 \lesssim 10^4$ Mpc) re-enter the Hubble radius during either radiation or the matter domination. To explain the causal connection between different modes, these modes should be well inside the Hubble radius at the very early stage of the universe, i.e., $\lambda_p < H^{-1}$. This will be possible, if we have an epoch in the early universe during which these length scales increases faster than the Hubble radius as we go forward in time, i.e.,

$$\frac{d}{dt}\left(\frac{\lambda_p}{H^{-1}}\right) > 0 \tag{3.2}$$

which eventually leads to

$$\ddot{a} > 0 \tag{3.3}$$

In nutshell, the universe has to go through a phase of accelerated (inflationary) expansion during the early universe which would account for the generation of the primordial fluctuations. In Fig. 2.3, if we include the condition (3.3) then H^{-1} behaves as a^{n} where n is smaller than 1 during the inflationary phase. In Fig. 3.1, we illustrated the evolution of the Hubble radius and perturbation scales during inflation and radiation/matter epochs. It is

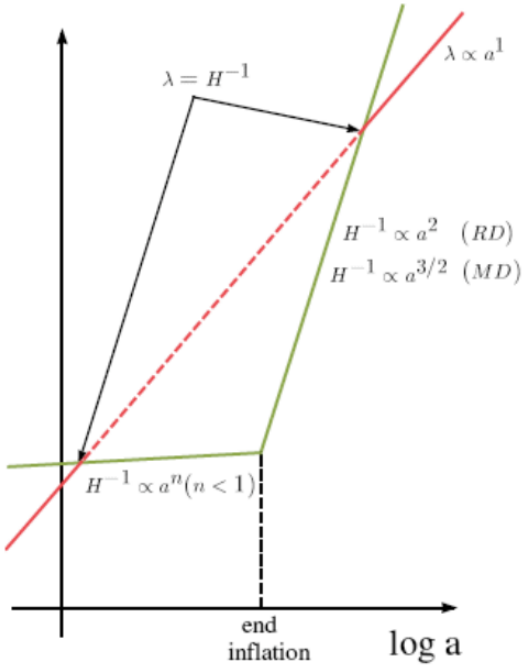

Figure 3.1: The Hubble radius (green) and a perturbation scale λ (red) vs a scale factor in the standard inflationary model. Ref. [25]

quite evident that modes leaving the Hubble radius during the late phase of inflation, would not be well inside the Hubble radius during the early epoch of the universe unless we have inflation.

3.1 Resolving the horizon problem

In order to resolve the horizon problem, we assume that the universe underwent exponential inflation from time t_i to t_f. Let H[1] be the constant during the inflation and A be the extent by which a scale factor increased during the inflationary phase. For $A \gg 1$, horizon's expansion has dominating contribution at the decoupling and then, the length of the forward light cone be

$$l_I(t_{dec}, 0) = a_{dec} \int_0^{t_{dec}} \frac{1}{a(t')} dt' \simeq \left(\frac{a_{dec}}{H}\right) \left(\frac{t_{dec}}{t_f}\right)^{1/2} A, \tag{3.4}$$

[1] As we have from the condition of the inflation that ρ+3p<0. We assume an extreme condition when ρ = -p and this would eventually lead to inflation and is known as de-Sitter inflation.

where $t_i \simeq H^{-1}$. Therefore, the ratio of the forward to the backward light-cone is (using $H \simeq 10^{13}$GeV)

$$R_I = \left(\frac{l_B}{l_F}\right) \simeq \left(\frac{A}{10^{26}}\right) \tag{3.5}$$

For $R_I \simeq 1$, $A \simeq 10^{26}$. Therefore, the scale factor increases by 10^{26}. Change in scale factor is expressed using N (number of e-folds) and is defined as

$$N = \int_{t_i}^{t} H dt = ln\left(\frac{a(t)}{a_i}\right) \tag{3.6}$$

Therefore,we need about 60 e-folds of inflation (Since N = ln$(a_f/a_i) \simeq 60$) to overcome the horizon problem.

3.2 Resolving the flatness problem

Inflation resolves the flatness problem elegantly. As the Hubble parameter is constant during inflation, therefore,

$$|\Omega - 1| = \frac{|K|}{a^2 H^2} \propto \frac{1}{a^2} \tag{3.7}$$

We assume that the start of radiation phase is the end of the inflation, where $|\Omega - 1| \simeq 10^{-60}$. Using eq. (3.6), one can write

$$\frac{|\Omega - 1|_{t=t_f}}{|\Omega - 1|_{t=t_i}} = \left(\frac{a_i}{a_f}\right)^2 = e^{-2N} \tag{3.8}$$

which means $|\Omega - 1|_t$ decreases as e^{-2N} till the end of the inflation (Fig. 3.2). It requires about 60 e-folds in order to resolve the horizon problem.

3.3 Inflation and the inflaton

In the above two-section, we saw how inflation resolves the horizon and flatness problems. However, we still need to answer a question: what is responsible for the inflation at the early times? It cannot be the cosmological constant (Λ), because a universe dominated by vacuum energy stays dominated by it for the infinite future. Since in de-Sitter background radiation and matter-energy density decreases exponentially, we will never have radiation and matter

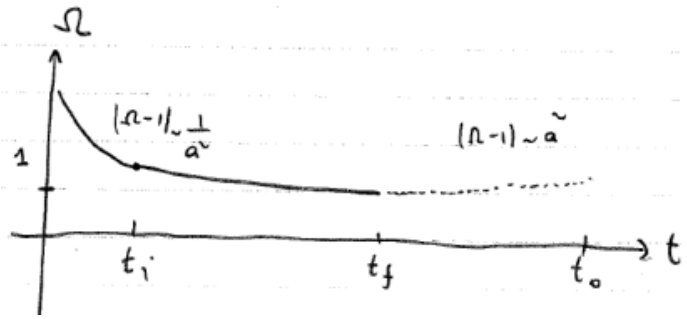

Figure 3.2: Illustration of the flatness problem's solution where $|\Omega - 1|$ decreases as exponentially till the end of the inflation and then increases as for the radiation/ matter epoch to match the current value, i.e. $|\Omega - 1|_{t=t_o} \simeq 1$ Ref. [25]

domination [27]. In high energy physics, scalar fields are often used, that can help us in driving inflation. Consider a canonical scalar field ϕ (known as inflaton), described by V(ϕ). Action (3.9.a) and the stress-energy tensor (3.9.b) of such field are

$$S[\phi] = \int d^4x\sqrt{-g}\left[\left(\frac{1}{2}\right)(\partial_\mu\phi\partial^\mu\phi) - V(\phi)\right] \tag{3.9.a}$$

$$T^\mu_\nu = \partial^\mu\phi\partial_\nu\phi - \delta^\mu_\nu\left[\left(\frac{1}{2}\right)(\partial_\lambda\phi\partial^\lambda\phi) - V(\phi)\right] \tag{3.9.b}$$

Using the above action (3.9.a), one arrives at the Klein-Gordon equation

$$\ddot{\phi} + 3H\dot{\phi} + V_\phi = 0 \tag{3.10}$$

Being homogeneous and isotropic, the Friedmann background (2.1) implies that ϕ will be time dependent and the stress energy tensor would be diagonal and can be written in term of ϕ as follows

$$T^0_0 = \rho = \left[\left(\frac{\dot{\phi}^2}{2}\right) + V(\phi)\right], \tag{3.11.a}$$

$$T^i_j = -\rho\delta^i_j = -\left[\left(\frac{\dot{\phi}^2}{2}\right) - V(\phi)\right]\delta^i_j. \tag{3.11.b}$$

One finds the condition of inflation using the above expression for the ρ and p, i.e. $(\rho + 3p) < 0$

$$\dot{\phi}^2 < V(\phi) \tag{3.12}$$

which means inflation can be only achieved when the dominance of the potential energy prevails over the kinetic term.Friedmann equations eq. (2.5.a) and (2.5.b) reduce to

$$H^2 = \left(\frac{1}{3M_{\rm Pl}^2}\right)\left[\left(\frac{\dot{\phi}^2}{2}\right) + V(\phi)\right] \tag{3.13.a}$$

$$\dot{H} = -\frac{\dot{\phi}^2}{2M_{\rm Pl}^2} \tag{3.13.b}$$

Integrating above both equations in terms of cosmic time t we get [26]

$$\phi(t) = \sqrt{2}M_{\rm PI}\int dt\sqrt{(-\dot{H})} \tag{3.14.a}$$

$$V(t) = M_{\rm PI}^2(3H^2 + \dot{H}) \tag{3.14.b}$$

3.4 Slow roll inflation

The condition (3.3) that prevalence of the potential energy over the the kinetic energy of the inflaton is a must for inflation to happen. However, if the inflaton gradually rolls down the potential,

$$\dot{\phi}^2 \ll V(\phi) \tag{3.15}$$

then the inflation is guaranteed. In order to attain the required 60 or more e-folds of inflation, we ensure

$$\ddot{\phi} \ll (3H\dot{\phi}) \tag{3.16}$$

The above two conditions are popularly termed slow-roll approximation and they are used to construct analytical solutions for both background and the perturbations.

3.5 Slow roll parameters

Given a potential for an inflaton, slow roll approximation requires the following two dimensionless parameters to be less than unity in order to inflation to occur

$$\epsilon_V = \left(\frac{M_{\rm Pl}^2}{2}\right)\left(\frac{V_\phi}{V}\right)^2 \tag{3.17.a}$$

$$\eta_V = (M_{\rm Pl}^2)\left(\frac{V_{\phi\phi}}{V}\right) \tag{3.17.b}$$

where $V_{\phi\phi}$ is $d^2V/d\phi^2$. These are termed as the potential slow roll (PSR) parameters. One of the flaws is that these parameters do not take into consideration the field's dynamics. It does not impose any restriction on the kinetic energy of the field. To do this, we use ($3H\dot{\phi} = -V_\phi$) [26]. However, PSR parameters are useful. They assist in determining the domains and parameters that can lead to inflation for a given potential. The following definition of the slow roll parameter and higher order slow roll parameters are now more commonly used,

$$\epsilon_1 = -\frac{\dot{H}}{H^2} \text{ and } \epsilon_{i+1} = \frac{dln\epsilon_i}{dN} \tag{3.18}$$

By substituting (3.18) in the (3.13.b), we get

$$\frac{\ddot{a}}{a} = H(1-\epsilon_1) \tag{3.19}$$

This automatically leads to the condition on ϵ_1, i.e., it must be less than unity till the inflation is in the action. Once it becomes equal to unity, inflation ceases.

3.6 Background evolution

We will slightly modify our Friedmann equations (eq. 3.13.a, 3.13.b, 3.10) by changing the independent vairable from t and N ($dN = Hdt$) (3.6) and we get

$$H^2 = \frac{V(\phi)}{(M_{\rm Pl}^2)(3-\epsilon_1)} \tag{3.20.a}$$

$$\frac{dH}{dN} = -2\epsilon_1 H \tag{3.20.b}$$

$$\frac{d^2\phi}{dN^2} + (3-\epsilon_1)\left(\frac{d\phi}{dN}\right) + \frac{V_\phi}{H^2} = 0 \tag{3.20.c}$$

where eq. (3.22.b) is the Klein-Gordon equation and ϵ_1 (slow roll parameter) modifies to

$$\epsilon_1 = \frac{1}{2M_{\rm Pl}^2}\left(\frac{d\phi}{dN}\right)^2 \tag{3.21}$$

By utilizing the slow roll inflation (3.16), we can find the ϕ analytically, i.e.,

$$H^2 \simeq \frac{V(\phi)}{3M_{\rm Pl}^2} \tag{3.22.a}$$

$$\frac{d\phi}{dN} \simeq -\frac{V_\phi}{3H^2} \tag{3.22.b}$$

3.7 Model: Quadratic potential

We will explore the quadratic model in this section, as well as plot and compare the evolution of the inflaton, H, ϵ_1 with the analytical solution.
This model has the following form,

$$V(\phi) = \frac{1}{2}m^2\phi^2 \tag{3.23}$$

Upon using (3.10), we get

$$\frac{d\dot{\phi}}{d\phi} = -\frac{\dot{\phi}\sqrt{(\frac{3}{2M_{\rm PI}^2})(\ddot{\phi} + m^2\phi^2)} + m^2\phi}{\dot{\phi}} \tag{3.24}$$

For the case when kinetic energy of the inflaton is dominating over potential energy, we find that (for the case $\phi > 0$, $\dot{\phi} < 0$)

$$\frac{d\dot{\phi}}{d\phi} \simeq \sqrt{\frac{3}{2M_{\rm PI}^2}}\dot{\phi} \tag{3.25}$$

The solution of this equation is

$$\dot{\phi} = Ce^{\sqrt{\frac{3}{2M_{\rm PI}^2}}\phi} \tag{3.26}$$

where $C < 0$ is constant. This equation shows that velocity of inflaton decreases exponentially more quickly than decrease in inflaton value. Therefore, the case of dominating kinetic energy gets damped within a short interval and the trajectory in the phase plot meets attractor. This substantially enlarges the set of the initial condition which leads to an inflationary stage [28]. Once the trajectory joins the attractor (Fig. 3.3), we use slow roll condition ($3H\dot{\phi} \simeq -V_\phi$) get that

$$\dot{\phi}_{atr} \approx -\sqrt{\frac{2}{3}}mM_{\rm Pl} \tag{3.27}$$

We will utilize the eq. (3.22.a) and (3.22.b) to evaluate the analytical form for the inflaton (ϕ), Hubble parameter(H) , and the slow roll parameter(ϵ_1) and we get

$$\phi^2 \simeq \phi_i^2 - 4M_{\rm Pl}^2N \tag{3.28.a}$$

$$H^2 \simeq \frac{m^2}{6}\left[\left(\frac{\phi_i}{M_{\rm Pl}}\right)^2 - 4N\right] \tag{3.28.b}$$

$$\epsilon_1 \simeq \frac{2}{\phi_i^2 - 4M_{\rm Pl}^2N} \tag{3.28.c}$$

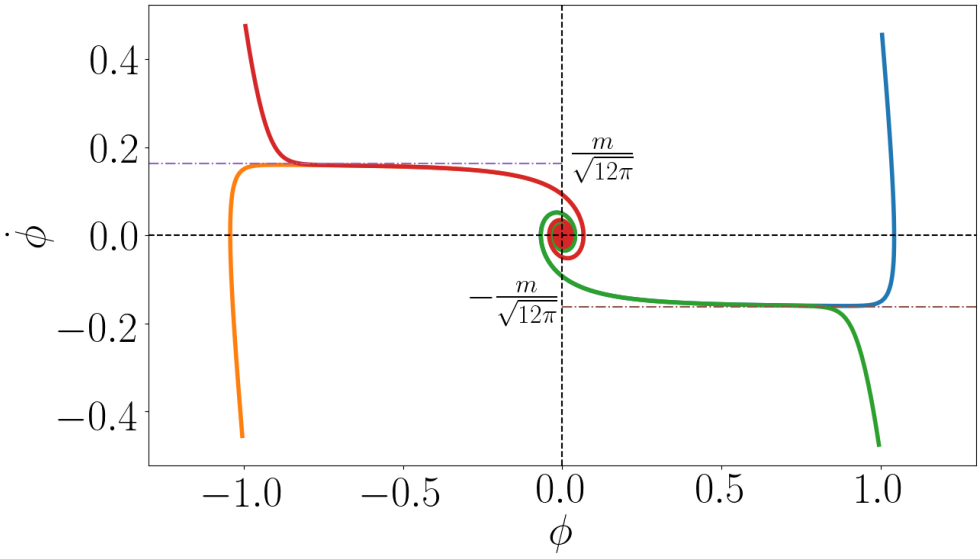

Figure 3.3: Phase-space plot ($\dot{\phi}$-ϕ) of the quadratic potential (3.23). For this, we have used m=1 and G=1. The attractor solution is mentioned in eq. (3.27). (Plotted in python by using a self-written code for the background evolution).

In order to compare the analytical and numerical solution for the above three parameters, we used the value of ϕ_i = 16.5 $M_{\rm Pl}$, m = 7.18$\times$ 10^{-6} $M_{\rm Pl}$, ϵ_{1i} = 7.346 $\times$ 10^{-3}, and N_e = 68.6 (e-fold value at the end of the inflation) from the ref. [29]. For coding purpose, $M_{\rm Pl}$ = 1 has been chosen.

As we can in figures (3.4*b*), (3.4*c*), and (3.4*d*) the numerical solution and analytical solution match well enough, this acts as a benchmark for the code used for the numerical evaluation.

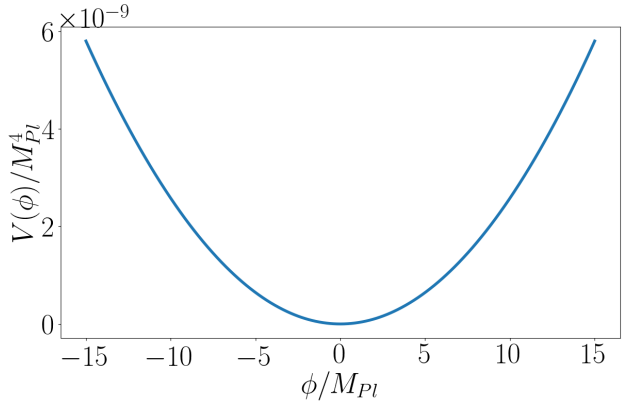

(a)
$V(\phi)$ vs ϕ

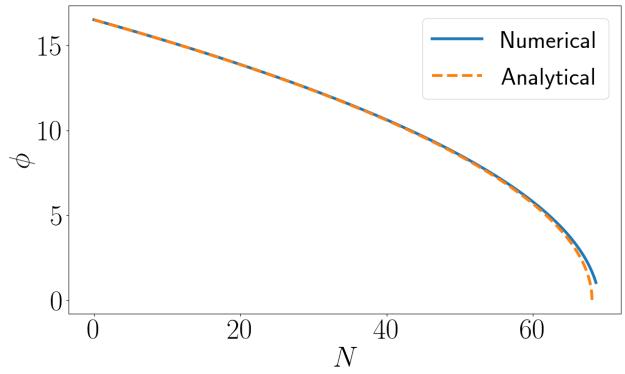

(b) ϕ **vs** N

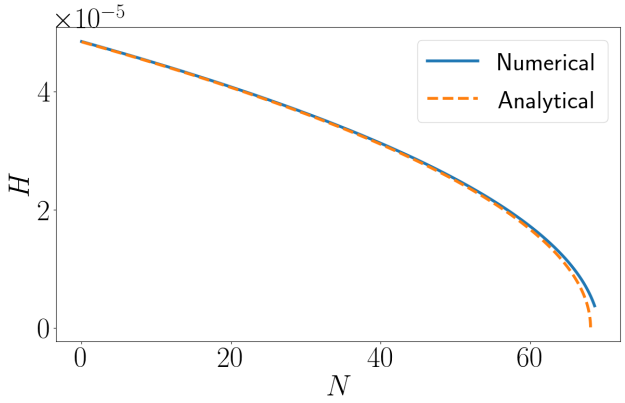

(c)
H vs N

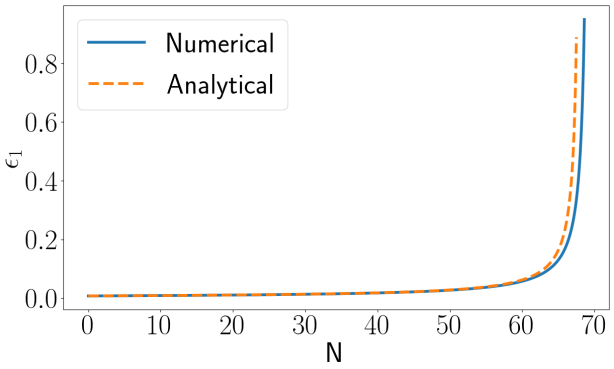

(d) ϵ_1 **vs** N

Figure 3.4: These are plots of the $V(\phi)$, ϕ, H, and ϵ_1. As we can see the numerical and analytical matches well except at the end where the slow roll approximation fails. (Plotted in python by using a self-written code for the background evolution).

Chapter 4

Generation of perturbation

Our universe is homogeneous, but only when averaged over large scales. Looking back in time till the last scattering surface, we find that the order of temperature inhomogeneity is of the order of 10^{-5}. Our current view of the universe's structure is that it originated with a small 'seed' perturbations that evolved through time to form all of the structures we see today. Our proposal for the perturbation's origin is quantum fluctuations during inflation in the early universe. It has generated both density perturbation and gravitational waves. They extend from very short scales to cosmological scales. We will depart from the homogeneity and isotropy that allow us to characterise different models in this chapter. We will deal with tiny perturbations, assuming that the perturbation's distribution is statistically homogeneous and isotropic [30].

4.1 Classification of the perturbation and gauge invariance

In a Friedmann background, the perturbation is decomposed according to how they behave on the hyperspaces of the constant time. This classify perturbations into three types: scalars, vectors, and tensors. Inhomogeneities and anisotropies in the universe are caused by scalar perturbations, which are invariant under spatial rotation. Vector perturbation transforms like a vector under rotation and they are generated by a rotational field or vorticity field. Tensor perturbation which behaves as a tensor under rotation is the reason for the gravitational waves generation without any source.

In a (D+1) dimensional spacetime, the perturbed metric tensor has two scalar (irrespective of the dimension we are in, (D-1) vector, and (D+1)(D-2)/2 tensor degree of freedom (DOF) (for detailed calculation refer ref. [26]). Overall we have D(D+1)/2 degrees of freedom for describing our perturbed metric in the FLRW background. So, for the case of the (3+1) dimensional spacetime, we have two scalar, two vectors, and two tensor degrees of freedom. Because the magnitude of these perturbations is supposed to be very small, we can describe them using linear perturbation theory, and it can be proved that in the linear order, all of these perturbations evolve separately. [31] [30] [26].

There would be one more point we would add that we have a comoving observer in the case of the FLRW background and it is special because with its respect the universe looks homogeneous and isotropic. But same is not true in the case of perturbations. Hence, there is no preferred reference frame for describing them. There is a variety of coordinate choices that exist. But we have to keep one point at the back of the mind that the metric and coordinates reduce to the background FLRW line element when perturbation goes zero. Gauge is such a choice of the coordinate that preserves the background FLRW. Going from one Gauge to another through co-ordinate transformation is known as Gauge transformation. There are two ways to deal with it: declare certain gauge-invariant quantities or pick a specific gauge and operate with it throughout. We will be adopting the latter approach for the following discussion [26]. The former approach can be found in the work of the ref. [32] [33].

4.2 Scalar perturbations

After accounting for the scalar perturbation in the background universe, our FLRW metric becomes [32]

$$ds^2 = (1+2A)\,dt^2 - 2a(t)\,(\partial_i B)\,dx^i dt - a^2(t)\,[\,(1-2\psi)\,\delta_{ij} + 2(\partial_i\partial_j E)]\,dx^i dx^j \tag{4.1}$$

As we can see we have four scalar, i.e., A, B, E, and ψ. But two can be eliminated through following infinitesimal co-ordinate transformations

$$t \to t + \delta t \;\; and \;\; x_i \to x_i + \partial_i(\delta x) \tag{4.2}$$

where δx and δt are function of space and time. Clearly, the metric (4.1) will not be invariant under above gauge transformation. So, in order to have the metric invariant, A, B,ψ, and E

transform as

$$A \to (A - \dot{\delta t}), \qquad B \to [B + \frac{\delta t}{a} - a\dot{\delta x}], \tag{4.3}$$

$$\psi \to (\psi - H\delta t), \qquad E \to E - \delta x. \tag{4.4}$$

We can choose the specific form of the δt and δx and restrict ourselves to a particular gauge. We can define two gauge invariant quantities - known as Bardeen potential in literature [34] [33]- which characterizes the two dof of the scalar perturbation as mentioned above and they are given as

$$\Phi = A + \frac{d}{dt}\left[a\left(B - a\dot{E}\right)\right] \quad and \quad \Psi = \psi - \left[aH(B - a\dot{E})\right]. \tag{4.5}$$

Two popular gauge that are used: the Newtonian gauge (B=0, E=0) and the spatial flat gauge (ψ=0, E=0). We will work in the Newtonian gauge. In this gauge, A = Φ and ψ = Ψ and hence, perturbed metric (4.1) looks like

$$ds^2 = (1 + 2\Phi)dt^2 - a^2(t)(1 - 2\Psi)\delta_{ij}dx^i dx^j \tag{4.6}$$

The Einstein equation can be separated into background and perturbed part at linear order, i.e.,

$$G^\mu_\nu = \bar{G^\mu_\nu} + \delta G^\mu_\nu \quad and \quad T^\mu_\nu = \bar{T^\mu_\nu} + \delta T^\mu_\nu \tag{4.7}$$

where $\bar{G^\mu_\nu}$ and δG^μ_ν are background Einstein tensor and the perturbed Einstein tensor respectively. Similarly, $\bar{T^\mu_\nu}$ and δT^μ_ν are background stress-energy tensor and the perturbed stress-energy tensor respectively. As we know background universe follow $\bar{G^\mu_\nu}$ = $\bar{T^\mu_\nu}$, therefore,

$$\delta G^\nu_\mu = 8\pi G \delta T^\nu_\mu \tag{4.8}$$

The perturbed Einstein tensor's components for the line element (4.6) are

$$\delta G^0_0 = -6H\left(\dot{\Psi} + H\Phi\right) + (\frac{2}{a^2})\nabla^2\Psi, \tag{4.9.a}$$

$$\delta G^0_i = 2\nabla_i(\dot{\Psi} + H\Phi), \tag{4.9.b}$$

$$\delta G^i_j = -2[\ddot{\Psi} + H(3\dot{\Psi} + \dot{\Phi}) + (2\dot{H} + 3H^2)\Phi + (\frac{1}{a^2})\nabla^2(\Phi - \Psi)]\delta^i_j + (\frac{1}{a^2})\nabla^i\nabla_j(\Phi - \Psi). \tag{4.9.c}$$

Scalar fields and ideal fluids with no vorticity are assumed to be the sources of the perturbations. At the linear order, these scalar fields and fluids do not posses any anisotropic stress. Under this condition, the perturbed stress-energy tensor looks like

$$\delta T^0_0 = \delta\rho, \quad \delta T^0_i = \nabla_i(\delta\sigma), \quad \delta T^i_j = -\delta p\delta^i_j, \tag{4.10}$$

where $\delta\rho$, $\delta\sigma$, and δp are the perturbation in the energy density, energy flux, and the pressure respectively. In the absence of anisotropic stresses, $\Phi = \Psi$, as proved by eq. (4.9.c). As a result, we have

$$-3H\left(\dot{\Phi} + H\Phi\right) + \left(\frac{1}{a^2}\right)\nabla^2\Phi = (4\pi G)\,\delta\rho, \tag{4.11.a}$$

$$\nabla_i\left(\dot{\Phi} + H\Phi\right) = (4\pi G)\,\nabla_i\left(\delta\sigma\right) \tag{4.11.b}$$

$$\ddot{\Phi} + 4H\dot{\Phi} + \left(2\dot{H} + 3H^2\right)\Phi = (4\pi G)\,\delta p \tag{4.11.c}$$

$$\tag{4.11.d}$$

and using the equations (4.11.c) and (4.11.a) we obtain the following differential equation of Φ governing

$$\Phi'' + 3\mathcal{H}\left(1 + c_A^2\right)\Phi' - c_A^2\nabla^2\Phi + \left[2\mathcal{H}' + (1 + 3c_A^2)\mathcal{H}^2\right]\Phi \;=\; \left(4\pi G a^2\right)\delta p^{NA} \tag{4.12}$$

where $\Phi' = \partial\Phi/\partial\eta$, $\mathcal{H} = a'/a$ (conformal Hubble parameter), $c_A^2 = p'/\rho'$ (adiabatic speed of the perturbations), and $\delta p^{NA} = (\delta p - c_A^2\delta\rho)$ (non-adiabatic pressure).

To study the quantitative implications of the above equation of motion, we introduce a gauge invariant quantity in term of Φ and cosmological parameters, known as curvature perturbation (R) [26]

$$\mathcal{R} = \Phi + \left(\frac{2\rho}{3\mathcal{H}}\right)\left(\frac{\Phi' + \mathcal{H}\Phi}{\rho + p}\right), \tag{4.13}$$

Upon using eq. (4.12) and background equations, one finds that $\mathcal{R}$ in Fourier space can be written as

$$\mathcal{R}'_k = \left(\frac{\mathcal{H}}{\mathcal{H}^2 - \mathcal{H}'}\right)\left[\,(4\pi G a^2)\delta p_k^{NA} - c_A^2 k^2\Phi_k\right] \tag{4.14}$$

It can be easily seen in the limit $k/aH = k/\mathcal{H} \;\ll 1$ (super Hubble scale), the term $c_A^2k^2\Phi_k$ can be neglected. Furthermore, non-adiabatic pressure is assumed to be zero in the case of a perfect fluid. (i.e. $\delta p^{NA} = 0$). Therefore, $\mathcal{R}'_k \;\simeq\; 0$. In the case of a scalar field, however, the equation is (4.22). In other words, on super Hubble scales, when the perturbation is adiabatic curvature perturbation $\mathcal{R}_k$ freezes when it is outside the Hubble radius.

4.3 Vector perturbations

The FLRW metric is written as (after including the vector perturbation [32]),

$$ds^2 = dt^2 - 2a(t)(S_i)dx^i dt - a^2(t)[\delta_{ij} + (\nabla_i \mathcal{F}_j + \nabla_j \mathcal{F}_i)]dx^i dx^j \tag{4.15}$$

By choosing a particular gauge where S_i = 0 and $\mathcal{F}_i \propto F_i$ (a divergence free vector), It is possible to derive the components of a perturbed Einstein tensor and they are as

$$\delta G_0^0 = 0 \tag{4.16.a}$$

$$\delta G_i^0 = \left(\frac{1}{2}\right)(\nabla^2 \dot{F}_i) \tag{4.16.b}$$

$$\delta G_j^i = -\left(\frac{1}{2}\right)[3H(\nabla_i \dot{F}_j + \nabla_j \dot{F}_i) + (\nabla_i \ddot{F}_j + \nabla_j \ddot{F}_i)] \tag{4.16.c}$$

$$\tag{4.16.d}$$

In absence of the vector sources, δG_i^0 and δG_j^i become zero. Hence, equating them equal to zero would lead to F_i = 0. It means in absence of vector sources, the vector perturbations vanish identically.

4.4 Tensor perturbations

When the tensor perturbations are taken in account, the FLRW metric turns out to be

$$ds^2 = dt^2 - a^2(t)\left[\delta_{ij} + h_{ij}\right] dx^i dx^j \tag{4.17}$$

where h_{ij} is a symmetric, transverse and traceless tensor. As we have seen, there are two independent degrees of freedom, which correspond to two different types of gravitational wave polarization. We can write the perturbed Einstein tensor as follows:

$$\delta G_0^0 = 0 \tag{4.18.a}$$

$$\delta G_i^0 = 0 \tag{4.18.b}$$

$$\delta G_j^i = -\left(\frac{1}{2}\right)\left[\ddot{h}_{ij} + 3H\dot{h}_{ij} - \left(\frac{1}{a^2}\right)\nabla^2 h_{ij}\right] \tag{4.18.c}$$

$$\tag{4.18.d}$$

We obtain the differential equation related to the amplitude of the gravitational wave [32] in conformal time coordinate to be in the absence of aniostropic stress.

$$h''_{ij} + 2\mathcal{H}h'_{ij} - \nabla^2 h_{ij} = 0 \tag{4.19}$$

4.5 Generation of perturbations during inflation

One of the most striking characteristics of inflation is that it provides the mechanism for perturbation production [26]. It is the quantum fluctuation related to inflation that grows and leads to inhomogeneities and anisotropies. The level of inhomogeneity in the CMBR and the structure formation are determined by the curvature perturbation term, which is proportional to the Bardeen potential. Using the perturbed Einstein equation, we will try to find the equation of motion for the curvature perturbation term. Then, we will quantize the curvature and tensor perturbations. This will help in imposing vacuum initial conditions on the various Fourier modes of the perturbations when they are well inside the Hubble radius at the early epoch.

4.5.1 The curvature perturbation's ($\mathcal{R}$) equation of motion

The perturbation in the assumed scalar field is $\delta\phi$. The perturbed stress energy tensor

$$\delta T^0_0 = (\dot{\phi}\dot{\delta\phi} - \dot{\phi}^2\Phi + V_\phi\delta\phi) = \delta\rho, \tag{4.20.a}$$

$$\delta T^0_i = \nabla_i(\dot{\phi}\delta\phi) = \nabla_i(\delta\sigma), \tag{4.20.b}$$

$$\delta T^i_j = -(\dot{\phi}\dot{\delta\phi} - \dot{\phi}^2\Phi - V_\phi\delta\phi)\delta^i_j = -\delta p\delta^i_j. \tag{4.20.c}$$

Because there is no anisotropic stress in the scalar field, therefore, $\Phi = \Psi$. On substituting the values of $\delta\rho$, $\delta\sigma$, and δp from equations (4.20.a), (4.20.b), and (4.20.c) into equations (4.9.a), (4.9.b), and (4.9.c) , we get

$$\Phi'' + 3\mathcal{H}(1 + c_A^2)\Phi' - c_A^2\nabla^2\Phi + [2\mathcal{H}' + (1 + 3c_A^2)\mathcal{H}^2]\Phi = (1 - c_A^2)\nabla^2\Phi \tag{4.21}$$

Upon comparing with eq. (4.12), we get

$$\delta p^{NA} = \left(\frac{1 - c_A^2}{4\pi G a^2}\right)\nabla^2\Phi \tag{4.22}$$

In this case, $\mathcal{R}_k$ simplifies to

$$\mathcal{R}'_k = -\left(\frac{\mathcal{H}}{\mathcal{H}^2 - \mathcal{H}'}\right)(k^2\Phi_k) \tag{4.23}$$

Again differentiating the above equation and using the definition of curvature perturbation (4.14), Bardeen potential (4.12), and background equations, we obtain the differential equation of $\mathcal{R}_k$ which governs the evolution of the curvature perturbation to be

$$\mathcal{R}''_k + 2\left(\frac{z'}{z}\right)\mathcal{R}'_k + k^2\mathcal{R}_k = 0 \tag{4.24}$$

where z is defined as $(a\dot{\phi}/H)$ = $(a\phi'/\mathcal{H})$ and is completely dependent on the background quantities. The Mukhanov-Sasaki variable v [26] is defined as v = $\mathcal{R}z$. Substituting the definition of v in eq. (4.24), we obtain a differential in term of the Fourier modes of v as

$$\nu''_k + \left[k^2 - \left(\frac{z''}{z}\right)\right]\nu_k = 0 \tag{4.25}$$

4.5.2 Quantization of the perturbations

Because the Friedmann background is homogeneous and isotropic, we can write $\mathcal{R}$ in terms of the Fourier modes as

$$\hat{\mathcal{R}}(\eta, \vec{x}) = \int \frac{d^3\vec{k}}{(2\pi)^{3/2}}\left[\hat{a}_k\mathcal{R}_k(\eta)e^{i\vec{k}.\vec{x}} + \hat{a}^\dagger_k\mathcal{R}^*_k(\eta)e^{-i\vec{k}.\vec{x}}\right] \tag{4.26}$$

where $\hat{a}_k$ and $\hat{a}^\dagger_k$ are the creation and annihilation operator, which follow the commutation relation. At the linear order perturbation theory, it is the two-point correlation function that specifies the power spectrum and statistical behaviour of the perturbation. Perturbations are Gaussian in nature at the linear order. The power spectrum is described this way:

$$\int_0^\infty dlnk\,\mathcal{P}_s(k) = \int \frac{d^3(\vec{x} - \vec{x}')}{(2\pi)^3}\langle 0|\hat{\mathcal{R}}(\eta, \vec{x})\hat{\mathcal{R}}(\eta, \vec{x}')|0\rangle e^{-i[\vec{k}.(\vec{x}-\vec{x}')]} \tag{4.27}$$

where $\hat{a}_k|0\rangle$ = 0 for all k values. Using the above definition, we get scalar power spectrum as

$$\mathcal{P}_s(k) = \left(\frac{k^3}{2\pi^2}\right)|\mathcal{R}_k|^2 = \left(\frac{k^3}{2\pi^2}\right)\left(\frac{v_k}{z}\right)^2 \tag{4.28}$$

This approaches to a constant value when it reaches the super Hubble scale. Similarly for tensor perturbation, eq. (4.17) we define $u = ah$ and in the Fourier space it behaves as

$$u_k'' + \left[k^2 - \left(\frac{a''}{a}\right)\right] u_k = 0 \tag{4.29}$$

Eq. (4.25) and (4.29) are known as Mukhanov- Sasaki equation. Similar to scalar power spectra, tensor power spectra is defined as

$$\mathcal{P}_T(k) = 2\left(\frac{k^3}{2\pi^2}\right)|h_k|^2 = \left(\frac{k^3}{2\pi^2}\right)\left(\frac{u_k}{a}\right)^2 \tag{4.30}$$

We define scalar spectral index ($n_{\rm s}$), tensor spectral index ($n_{\rm T}$), and tensor-to-scalar ratio (r) as quantities that are related to observations. They are as follows:

$$n_s = 1 + \left(\frac{d\,ln\mathcal{P}_s}{d\,lnk}\right), \qquad n_T = \left(\frac{d\,ln\mathcal{P}_T}{d\,lnk}\right), \qquad r = \frac{\mathcal{P}_T(k)}{\mathcal{P}_s(k)} \tag{4.31}$$

When a mode crosses the Hubble radius ($k = aH$), the parameters listed above are examined. On the CMB scale, we will also discuss the limits on both parameters.

4.5.3 The Bunch Davies initial condition

We place some initial conditions on different modes of the perturbations when the modes are well inside the Hubble radius (at very early times).. As seen in eq. (4.29) and eq. (4.25), in sub-Hubble domain $k/(aH) \gg 1$, u_k and v_k behave as $e^{\pm(ik\eta)}$. Because the scalar and tensor perturbations are in vacuum in the initial state, just a positive frequency must be chosen and symptomatic form of the initial conditions are.

$$\lim_{(k/aH)\to\infty} (\nu_k(\eta),\, u_k(\eta)) \quad \to \quad \left(\frac{1}{\sqrt{2k}}\right) e^{-ik\eta} \tag{4.32}$$

4.5.4 Slow roll inflation power spectrum and observational constraints on CMBR

In the super-Hubble limit, the power spectrum of the scalar and tensor perturbation behaves as [35] [26] [25]

$$\mathcal{P}_s(k) \simeq \left(\frac{H^2}{2\pi\dot{\phi}}\right)^2 \tag{4.33}$$

$$\mathcal{P}_T(k) \simeq \left(\frac{8}{M_P^2}\right)\left(\frac{H}{2\pi}\right)^2 \tag{4.34}$$

The CMBR temperature anisotrpies has been measured with high accuracy by Planck satellite [36]. The power spectrum can be parameterised with two free parameters as

$$\mathcal{P}_s = A_s \left(\frac{k}{k_*}\right)^{n_s - 1} \tag{4.35}$$

According to current observations, $As \simeq 2.092 \times 10^{-9}$ [36] , which is known as COBE normalisation [26], which is the amplitude of the mode (termed as pivot scale $k_* = 0.05\,\mathrm{Mpc}^{-1}$), leaves the Hubble radius nearly 50 e-folds before the end of the inflation. According to the analysis of CMB data $n_s \simeq 0.9626 \pm 0.0057$ and r < 0.43 [36].

Chapter 5

Numerical approach for evaluation of the scalar power spectrum

In the models where it is not possible to find the analytical behaviour of the background and the perturbations, we employ numerical methods for the evaluation. As we have seen the scalar and tensor perturbations depend on the background variables, we will first evaluate it by using eq. (3.20.a) and (3.22.b). The field is assumed to start on the inflationary attractor when solving these equations. The inflaton's initial state is set to require 60 or so e-folds before the inflation is terminated.

For further discussion, we will restrict ourselves to scalar perturbations. To solve for the curvature perturbation, we can modify eq. (4.24), i.e., evolution of the $\mathcal{R}_k$, by expressing t time as N e-folds and rewriting it as

$$\frac{d^2\mathcal{R}_k}{dN^2} + \left(1 - 2\epsilon_1 + 2\frac{z_N}{z}\right)\frac{d\mathcal{R}_k}{dN} + \left(\frac{k}{aH}\right)^2 \mathcal{R}_k = 0 \tag{5.1}$$

where z_N is defined as dz/dN and $z = a\, d\phi/dN$. This equation will dictate how the curvature perturbation will evolve with increasing N values. Now, we need to set the initial condition. We defined the Bunch Davies initial condition when a mode is well inside the Hubble radius, i.e., $k/aH \gg 1$, as we have seen. For the same $N = N_{ic}$. The initial condition on $\mathcal{R}_k$ is

$$\mathcal{R}_k(N_{ic}) = \frac{1}{z(N_{ic})}\frac{1}{\sqrt{2k}} \tag{5.2}$$

$$\mathcal{R}'_k(N_{ic}) = -\mathcal{R}_k(N_{ic})\left\{1 + \frac{\phi_{NN}(N_{ic})}{\phi_N(N_{ic})}\right\} + i\sqrt{\frac{k}{2}}\frac{1}{Z(N_{ic})a(N_{ic})H(N_{ic})} \tag{5.3}$$

where $\phi_N = d\phi/dN$ and $\phi_{NN} = d^2\phi/dN^2$.

The perturbation will evolve from N_{ic} ($k/aH \gg 1$, known as sub-Hubble) to N_{shs} ($k/aH \ll 1$, known as super-Hubble). But implying this numerically, it is impossible. Therefore, numerically we take $k/aH = 10^2$ for the sub-Hubble and $k/aH = 10^{-5}$ for the super-Hubble. Apart from specific cases, it is found that once outside the Hubble radius, the amplitude of the $\mathcal{R}_k$ freezes to a constant value. This is evident in fig. (5.1), where we have plotted the real and the imaginary part of the $\mathcal{R}_k$ for k = 0.05 Mpc^{-1} when it comes to the quadratic potential.

There is one more ingredient we will feed for determining the perturbation. As we can see in eq. (5.2), we need to find $z(N)$. But z contains "a" scale factor, we can prove that

$$a_i = \frac{k_p}{e^{(N-N_*)}\, H(N - N_*)} \tag{5.4}$$

where k_p = 0.05 Mpc^{-1} is pivot scale at which the amplitude of scalar perturbation is known through observations. N_* is the e-fold value such that k_p crosses Hubble radius at $N_{\mathrm{end}} - N_*$ e-folds.

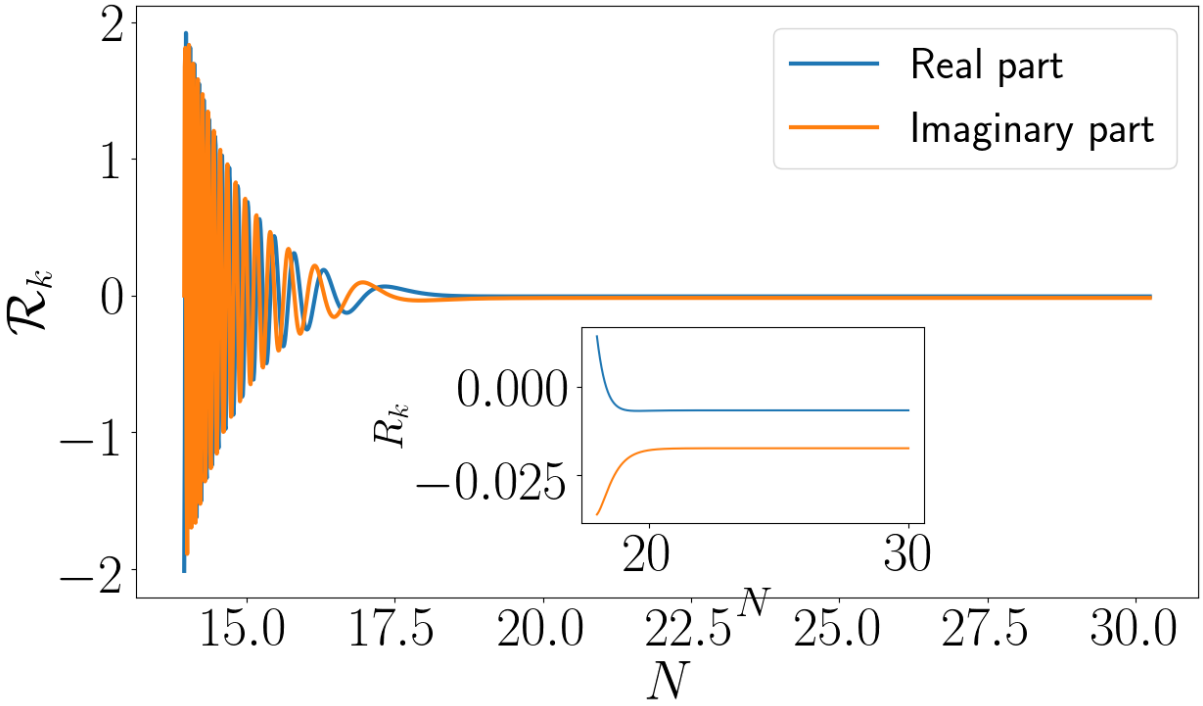

Figure 5.1: The evolution of the real and imagined parts of R_k for the quadratic potential (k = 0.05 Mpc^{-1}). (Evaluated using a self written code).

Let's discuss about the code that was used to compute the background quantities. The Klein-Gordan equation was solved using Python code. To evaluate the field values at different N e-folds values, we used the RK4 method [37]. We then used the background data to compute the scalar power spectrum for various Fourier modes using the inbuilt solver (SciPy). The code is model-agnostic and can be used with any single field or canonical scalar field. For all numerical analysis, $M_{\rm Pl}$ is set to be unity.

5.1 Quadratic potential

We are considering the potential of the inflaton of the form

$$V = \frac{m^2}{2}\phi^2 \tag{5.5}$$

Based on the COBE normalization [38], we find that the parameter m = 7.18 $\times$ 10^{-6} $M_{\rm Pl}$. In order to determine the power spectrum, we have chosen the initial values of field and slow roll parameter as ϕ_i = 16.5 $M_{\rm Pl}$ and ϵ_{1i} = 7.346×10^{-3}, respectively. According to the ref. [29], the end of inflation occurs after 68.6 e-folds, and the k_p = 0.05 Mpc^{-1} exits the Hubble radius 50 e-folds (N_*) before the end of inflation.

In fig. (5.2), we can see that power spectrum, computed numerically and analytically (eq. (4.33)), are separated by on y-axis (0.5 in log scale) and the slope differs by 0.0124. These differences are very small and evidently, the analytical and numerical values are agreeing very well.

5.2 Small field potential

We choose potential of the form

$$V(\phi) = V_o\left[1 - \left(\frac{\phi}{\mu}\right)^q\right] \tag{5.6}$$

We will focus on the scenario where q= 2. On setting μ = 10 $M_{\rm Pl}$. We find that based on COBE normalization, V_o = 5.38×10^{-10} $M_{\rm Pl}^4$. The initial conditions are: ϕ = 1.6 $M_{\rm Pl}$ and ϵ_{1i} = 5.39×10^{-4}, and N_{end} = 68.4. From the ref. [29], the pivot scale k_p crosses 50 e-folds before

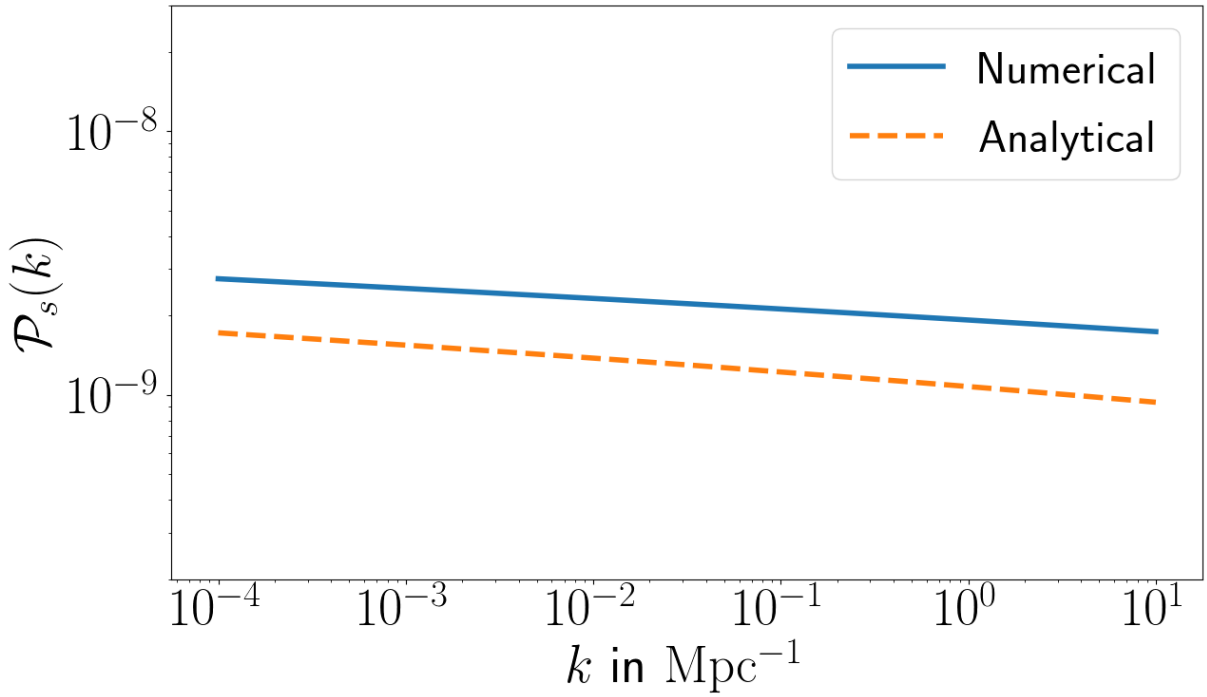

Figure 5.2: The quadratic potential's scalar power spectrum. (Evaluated using a self written code).

the end of inflation.

In fig. (5.3), the difference in the slope of the numerical and the analytical solutions is 0.0065. It is easily seen that both the solution are behaving well at the CMB scales.

5.3 Starobinsky Model

Till now, we have dealt with slow roll inflation, but now we have a potential which deviates from slow roll for a brief period. Here is a model described by Starobinsky [39]. A linear potential with an abrupt shift in slope is used to characterise it.

$$V(\phi) = \begin{cases} V_0 + A_+(\phi - \phi_o) \ for \ \phi > \phi_o, \\ V_0 + A_-(\phi - \phi_o) \ for \ \phi < \phi_o, \end{cases} \tag{5.7}$$

where $A_+ \neq$A$_-$. We call it SM. We utilise the smoothed version of the above potential [40]to perform the numerical analysis and it is given as

$$V(\phi) = V_o + \frac{1}{2}(A_+ + A_-)(\phi - \phi_o) + \frac{1}{2}(A_+ - A_-)(\phi - \phi_o)\tanh\left(\frac{\phi - \phi_o}{\Delta\phi}\right) \tag{5.8}$$

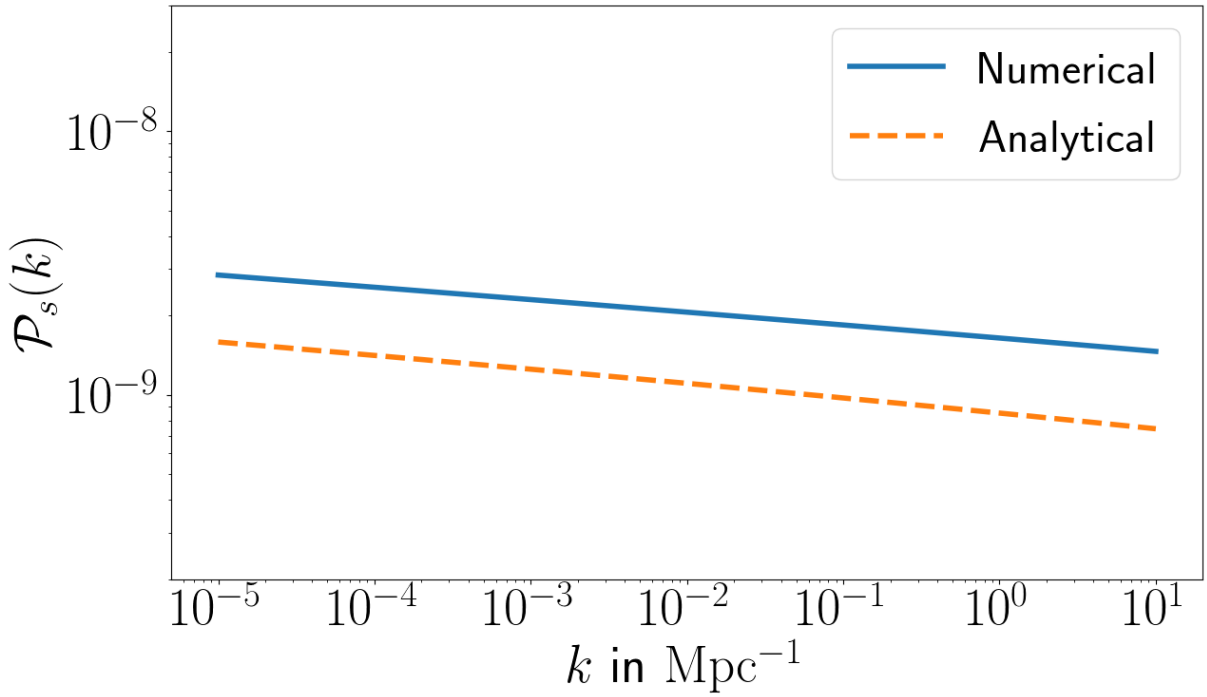

Figure 5.3: Power spectra for the small field potential (Evaluated using a self written code).

If we assume that V_o dominates, the first slow roll parameter (ϵ_1) will always be small. As can be seen, slow roll inflation has two stages, each with a brief break from the slow roll (fig. (5.4a)). This is represented in the large values of the second (ϵ_2) and third (ϵ_3) slow roll parameters in the figures (5.4b), (5.4c) when the inflaton passes ϕ_o. Because of the small value of ϵ_1, we can express the scalar power spectrum analytically [39]. The detailed analysis can be found in the reference [40]. It can be shown that the power spectrum for such model is

$$\mathcal{P}_s(k) \simeq A_s \Bigg\{ 1 - \frac{3\Delta A}{A_+}\frac{k_o}{k}\left[\left(1-\frac{k_o^2}{k^2}\right)\sin\left(\frac{2k}{k_o}\right) + \frac{2k_o}{k}\cos\left(\frac{2k}{k_o}\right)\right] + \frac{9^2}{2A_+^2}\frac{k_o^2}{k^2}\left(1+\frac{k_o^2}{k^2}\right)\left[1+\frac{k_o^2}{k^2} - \frac{2k_o}{k}\sin\left(\frac{2k}{k_o}\right) + \left(1-\frac{k_o^2}{k^2}\right)\cos\left(\frac{2k}{k_o}\right)\right]\Bigg\} \tag{5.9}$$

where $\Delta A = A_- - A_+$. When comparing the above spectrum to the CMB data, we multiply it by $(k/k_p)^{n_s-1}$ to account for the tilt. When one compare the best fit values of the parameters to CMB data, we get $A_s = 2.11 \times 10^{-9}$, $k_o = 6.34 \times 10^{-5}\ Mpc^{-1}$, $\Delta A/A_+$ = -0.074, n_s = 0.97 (taken from the ref .[39]).

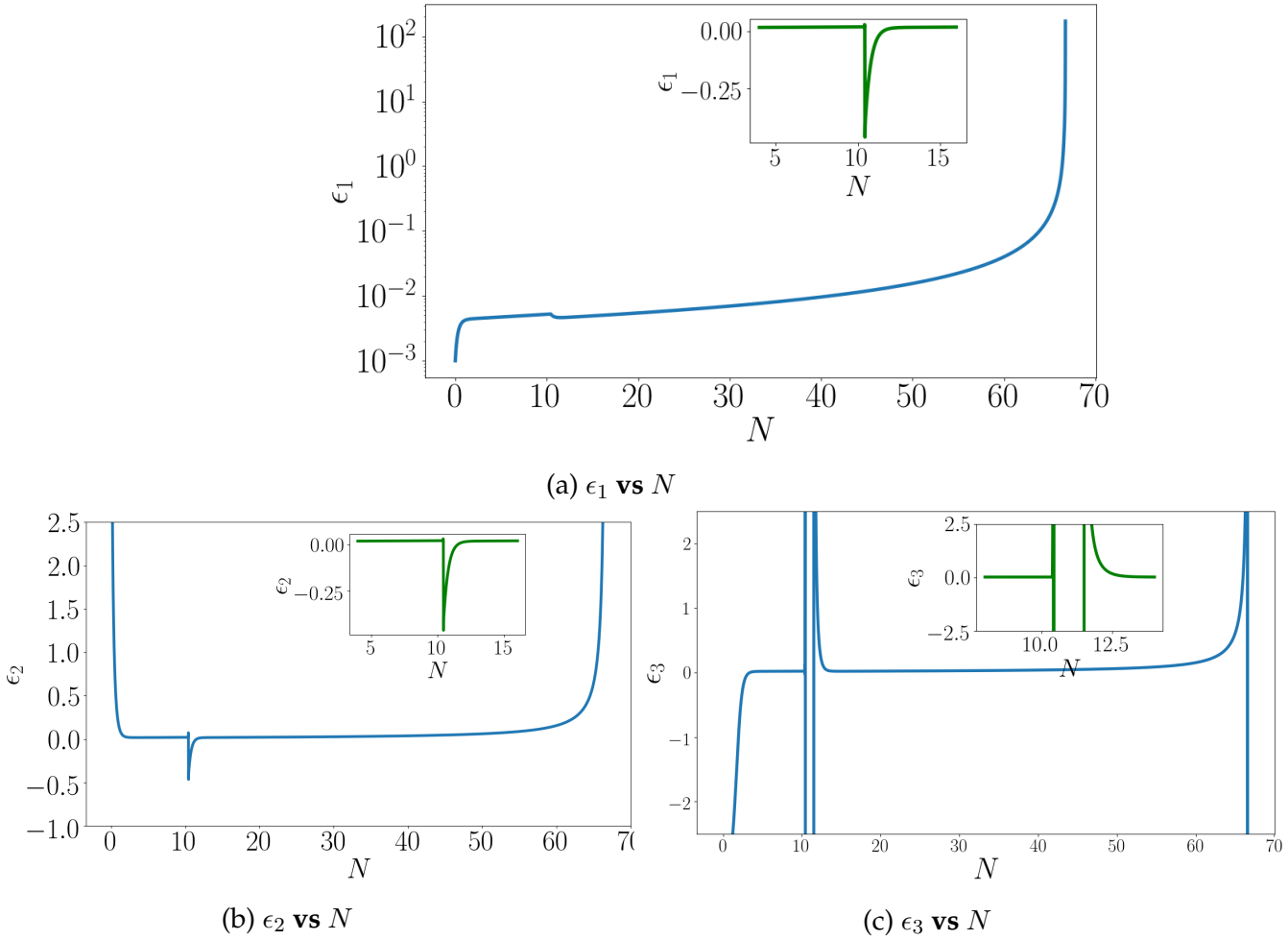

(a) ϵ_1 **vs** N

(b) ϵ_2 **vs** N

(c) ϵ_3 **vs** N

Figure 5.4: Plots of the first, second, and third slow roll parameters for the SM case. It is evident that ϵ_2 and ϵ_3 acquire very large values when it is crossing the ϕ_o. (Plotted in python by using a self-written code).

In fig. (5.5), we can see that the analytical and the numerical power spectra matches perfect ally and On large scales, it has a step-like feature, whereas on small scales, it is scale invariant.

Till now, we have tested our code with three potentials which are well established in the literature and our code is fine. Therefore, we have sufficient confidence in it. We will go ahead with it for studying potentials which would have non-trivial behaviour on small scales and would lead to formation of PBHs.

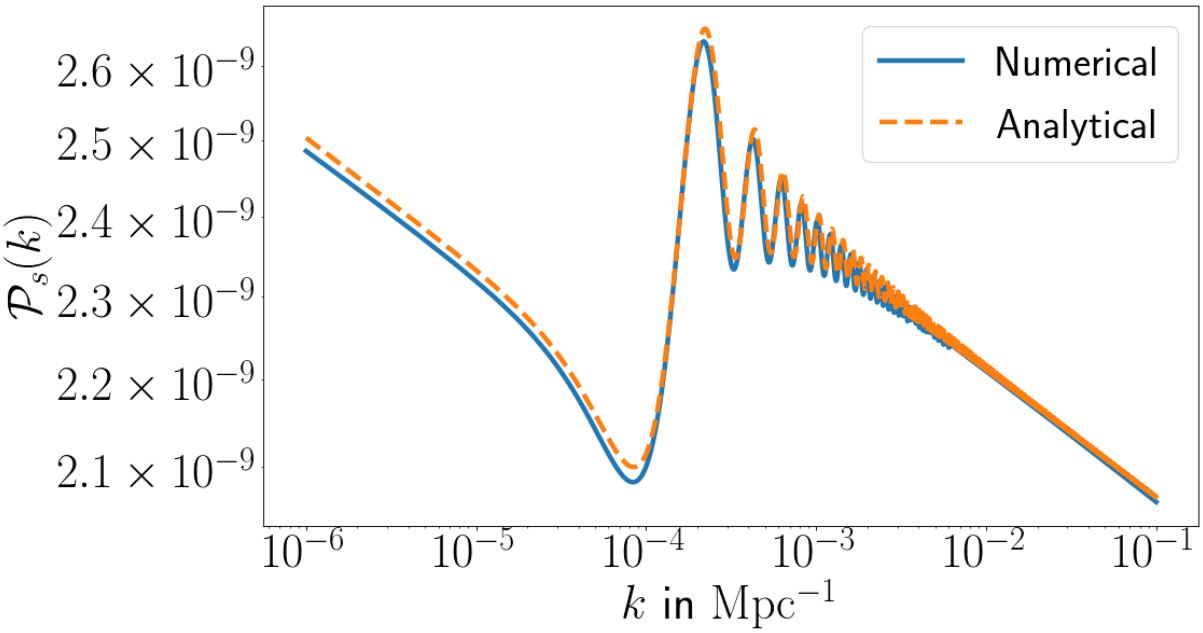

Figure 5.5: Power spectrum for the Starobinsky model. (Evaluated using a self written code).

Chapter 6

Formation of primordial black holes

The detection of gravitational waves from black hole binaries has revived interest in determining if such BHs might add to a strong candidate for cool dark matter (CDM). There are a few events that have been reported by the LIGO-VIRGO scientific collaboration [41] [42]. An interesting conclusion that emerges from the LIGO-VIRGO data analysis, is that such BHs are massive, with mass > $10M_{\odot}$, where $M_{\odot} = 2 \times 10^{33}$g (solar mass). In the present chapter, we will see how PBHs which originate in the early universe, can be generated through special initial conditions.

6.1 Cold dark matter and primordial black holes

As we know from the standard cosmology, how plasma and atoms-molecules came into existence post inflation. Further, it led to large-scale structure formation such as stars, galaxies, clusters, etc. We have to wait for nearly 100 million years to have the first stellar black hole (formed from the death of a massive star). Typically, a star with a mass of more than 3 $M_{\odot}$ would collapse to form an astrophysical black hole.

A black hole is a region of spacetime with very high curvature surrounded by a horizon sphere [43]. Usually, the radius of the black hole is defined using Schwarzschild radius, defined as

$$R_s = \frac{2GM}{c^2} \tag{6.1}$$

The possible range of the mass of the BHs are 10^{-5} kg to 10^{40} kg. Through observations, we found that black holes in binary systems have a range 3 $M_\odot$ to 160 $M_\odot$ (X-ray + GWs) and supermassive black holes have 10^6 $M_\odot$ to 10^{10} $M_\odot$ (galactic centre, AGN).

Ample evidence for the dark matter (DM) arises not only from the observations of the 'late' universe, such as galaxy clusters' observations, galactic rotation curves, and the bullet luster, but also from the growth of the perturbation between the CMBR formation and first galaxy formation, as well as the measurement of baryon-to-photon ratio from the Big Bang nucleosynthesis (BBN) (1 minute after the big bang) to the CMBR formation (400,000 years later). Hence, during the early universe dark matter must exist and therefore, stellar black hole cannot be a dark matter candidate. However, if we have BHs formed through the collapse of the hot dense plasma at very early times (before BBN), then, we have a potential candidate for the cold dark matter (CDM). They can form with any mass due to their primordial nature and are classified as non-baryonic, non-relativistic, and nearly collisionless. PBHs are thus seen as a one-of-a-kind non-baryonic contender for the CDM that is not bound by the BBN constraint.

6.2 Ultra slow roll

In chapter 1, we mentioned about the various mechanisms for the formation of the PBH, but for the current discussion, we will focus on the inflationary scenario only. During the radiation and matter dominance epochs, curvature perturbations (produced during inflation) re-enter the Hubble radius, forming PBHs. Majority of the inflationary models follow slow-roll inflation but they would not produce sufficient BHs for the astrophysical implications. As we have shown, the scalar power spectrum is bound on big scales (CMB scales), but it should be enhanced on small scales to have a considerable number of PBHs [44] [45]. This is possible if we deviate from the slow-roll inflation. We will identify such models where we start with slow roll but then deviate for a brief period and eventually return to slow roll before the inflation ends (fig. (6.1)).

To drive inflation with deviation from the slow roll, we consider an ultra-slow roll scenario where we will briefly depart from the slow roll. This can be done using a point of inflection in the potential. The point of inflection would cause an ultra-slow roll period,

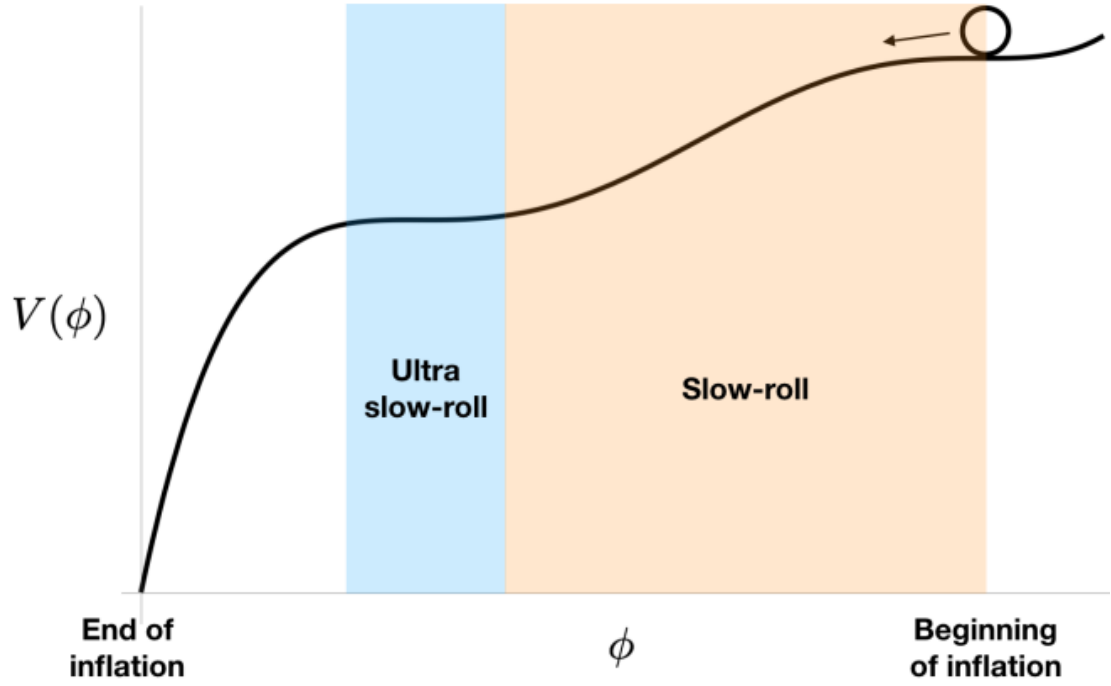

Figure 6.1: Example of how the field is rolling in a typical potential with a point of inflection. Ref. [45].

boosting the power spectrum for all modes leaving the Hubble radius during the same period. This can be divided into two categories where we violate inflation for a short period, known as punctuated inflation (PI) [44], and another where inflation is not violated, known as ultra slow-roll inflation (USR).

As we mentioned in ultra slow roll model, we have a point of inflection, i.e., $dV/d\phi = 0$ and $d^2V/d\phi^2 = 0$. Recall the equation of motion of the inflaton

$$\ddot{\phi} + 3H\dot{\phi} + \frac{dV}{d\phi} = 0 \tag{6.2}$$

For slow-roll inflation, we ignored the $\ddot{\phi}$ but if we use the same when we reach the inflection point, then, $\dot{\phi} = 0$. This implies that the field is not moving at all. This does not mean that the inflation has ended rather if it is not at the bottom of the potential, then, the potential energy will dominate and this is the case with the cosmological constant. Hence, we will have eternal de-Sitter expansion. But this is not what we see. [45]

If we do not ignore $\ddot{\phi}$, then, the equation of motion be

$$\ddot{\phi} + 3H\dot{\phi} = 0. \tag{6.3}$$

In this case, the field velocity decreases quickly as $\dot{\phi} \propto a^{-3} \propto e^{-3N}$ (upon solving eq. (6.3)). Hence, the potential energy dominates very quickly but $\dot{\phi}$ does not become zero because this helps the inflaton to pass through the flat potential to avoid eternal inflation and produce the inflaton perturbations. Note that the slow-roll parameter behaves as

$$\epsilon_1 = \frac{\dot{\phi}^2}{2M_{\rm Pl}^2 H^2} = \frac{1}{2M_P^2}(\frac{d\phi}{dN})^2 \propto a^{-6} \ll 1. \tag{6.4}$$

ϵ_1 is small and decreasing rapidly and this implies H is very close to constant. In a typical slow roll case, $\epsilon_{\rm V}$ and ϵ_1 can be used interchangeably but this is not true with USR as former becomes 0. In-fact, ϵ_1 dips during USR and higher order slow roll parameters (ϵ_2, and ϵ_3) do not follow slow roll behaviour rather they have very high values. This peculiar behaviour helps in recognizing the deviation from slow roll. We will further see this when we discuss various inflationary models.

6.3 Scalar power spectrum

As seen in chapter 4, we mentioned the analytical expression of the scalar power spectrum when a mode is crossing the Hubble radius and is expressed as

$$\mathcal{P}_s(k) \simeq \left(\frac{H^2}{2\pi\dot{\phi}}\right)^2 = \frac{H^2}{8\pi^2 M_{\rm Pl}^2 \epsilon_1} \tag{6.5}$$

where ϵ_1 is defined in eq. (6.4). This works properly for slow-roll inflation (shown in Chapter 5) but is partially true for ultra slow roll inflation. For slow-roll inflation, we saw how a mode freezes out once it crosses the Hubble radius but it is not true for ultra slow roll inflation. Rather one needs to evolve the perturbation till the ultra slow roll ends. It is quite evident that in ultra slow roll inflation, if we replace ϵ_1 with $\epsilon_{\rm V}$, then, the value of the scalar power spectrum would blow up and things would go bizarre

Recall in eq. (6.4), that ϵ_1 goes as a^{-6} and H is close to constant, consequently

$$\mathcal{P}_s \propto a^6 \propto e^{6N} \tag{6.6}$$

during ultra slow roll inflation. This means perturbation grows very fast during ultra slow roll. But it does not last long as if it does, then, $\mathcal{P}_s \to 1$. At this point, the perturbation

theory will break down and also it would lead to eternal inflation. This occurs when

$$\sqrt{\mathcal{P}_s} \simeq \frac{H}{\sqrt{\epsilon}} \simeq \frac{H}{\frac{\Delta\phi}{\Delta N}} \simeq 1 \tag{6.7}$$

Now, $\Delta\phi = H\Delta N$, that means during 1 e-fold field moves backwards (towards starting point) with scale H. So, the potential is moving up when it has to go down where inflation can end. Hence, inflation never stops. The typical value of the scalar power spectrum required for PBH formation, lies in the the range $\mathcal{P}_s \simeq 10^{-3} - 10^{-2}$ and it is independent of PBH mass and any potentially observable value of fraction of CDM in PBHs (A detailed calculation is shown in Appendix B).

6.4 PBH formation

PBH mass would be comparable to the horizon mass M_H (amount of mass within the Hubble radius). At the time of BBN, universe was dominated by the radiation and even after the inflation ends, it was same (inflaton reheated the universe by decaying into radiation). At the time of the radiation-matter equality, the horizon mass was on the order of $10^{16}\, M_\odot$. Therefore, we will focus on PBH formation during radiation domination when the Hubble mass was small.

As during radiation domination, background pressure was $\rho/3$ and in order to collapse mode k_{PBH} must have strong gravity to overcome the pressure and collapse to form a BH. Typical order of perturbation on CMB scale is (known as density contrast)

$$\delta = \frac{\delta\rho}{\rho} \simeq \mathcal{R}_k \simeq \sqrt{P_k} \simeq 5 \times 10^{-5} \tag{6.8}$$

which is very small for the formation of PBH. In order to form PBH, we need $\delta\rho/\rho \sim 1$ when a mode is re-entered into the Horizon. This can be done on small scales by proper choice of the initial conditions. It was in 1975, Bernard Carr [9] gave an estimate for the threshold value of δ using the Jean's length and Newtonian Gravity [45]. According to Carr,

$$\delta = \frac{\delta\rho}{\rho}_{k=aH} > \delta_c = c_s^2 \tag{6.9}$$

where c_s^2 is speed of the perturbation [46]. During radiation domination, $c_s = 1/\sqrt{3}$. But more recent simulations show that $\delta_c \simeq 0.45$. It is evident in the fig. (6.2), that once a mode

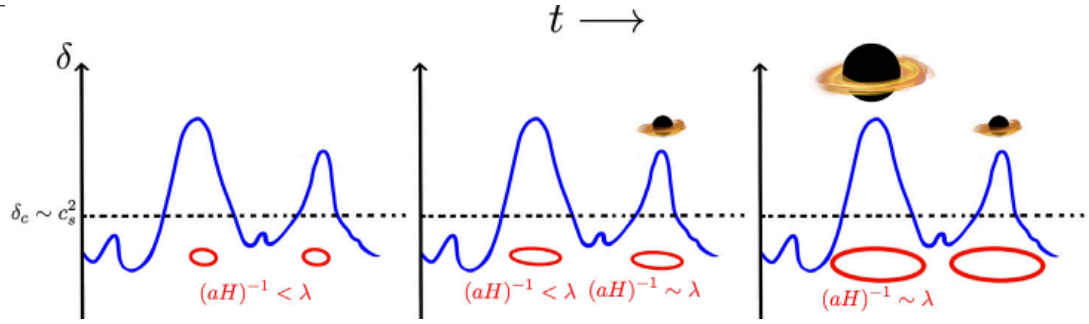

Figure 6.2: Sketch of how PBHs are formed when a k-mode with wavelength λ. When δ goes more than δ_c, perturbation collapse to form PBH. More heavy PBHs are formed by large λ or small k. Ref. [47]

having δ more than δ_c, re-enters the Hubble horizon, leading to a collapse forming a PBH. PBH mass is related to mass of the horizon at the time of the formation and it is related as

$$M_{PBH} = \gamma M_H = \gamma \frac{4\pi}{3} \frac{\rho}{H^3} \tag{6.10}$$

where γ is efficiency of the collapse. During radiation domination,

$$H^2 = \frac{8\pi G}{3}\rho = \frac{4\pi^3 G}{45} g_* T^4 \tag{6.11}$$

where g_* is relativistic degree of freedom and T temperature. Upon integrating above equation, one obtains

$$t = \left(\frac{4\pi^3 G}{45} g_*\right)^{-1/2} \frac{1}{2T^2} \tag{6.12}$$

Substituting this in eq. (6.10), one obtains

$$M_{PBH} = \gamma \frac{4\pi}{3} \frac{\rho}{H^3} = \gamma \frac{c^3 t}{G} \propto 2.03 \times 10^5 \gamma \left(\frac{t}{1s}\right) M_\odot \tag{6.13}$$

This puts a constraint on the mass of the PBH based on Hawking evaporation [48], i.e., the BH of mass 10^{15} g must have evaporated by now.

The Hubble parameter can be expressed in terms of redshift as [49]

$$H^2 = \Omega_{0r} H_0^2 (1+z)^4 \left(\frac{g_*}{g_{0*}}\right)^{-1/3} \left(\frac{g_*^s}{g_{0*}^s}\right)^{-4/3} \tag{6.14}$$

where g_{0*} = 3.38 and g_{0*}^s = 3.94 are the effective energy and the entropy degree of the freedom.

We will relate the mass of PBH with the horizon mass at the equality. Assuming, entropy and energy degree of freedom are equal at the matter-radiation equality ($\rho \propto g_*^{-1/3} a^{-4}$). One can prove using eq. (6.10) that (For proper proof see Appendix A)

$$M_{PBH} = \gamma\sqrt{2}\, M_{eq.} \left(\frac{g_*}{g_{eq.}}\right)^{1/6} \left(\frac{a}{a_{eq.}}\right)^2 \tag{6.15}$$

where a is defined at the time of the PBH formation. Using the relation, $k_{eq.} = a_{eq.} H_{eq.}$ and $k = aH$ ($k_{eq.}$ and k are modes).

$$M_{PBH} = \frac{\gamma}{\sqrt{2}}\, M_{eq.} \left(\frac{g_*}{g_{eq.}}\right)^{-1/6} \left(\frac{k}{k_{eq.}}\right)^{-2} \tag{6.16}$$

where M_{eq} = 5.83 $\times 10^{47}$ kg. As we can see, on small scales i.e., large k value would form smaller mass BHs whereas on large scales heavier mass BH can form. For the case of solar mass PBH, k_{PBH} ($\simeq 10^7\,\mathrm{Mpc}^{-1}$) collapses to form PBH.

As we have assumed at the re-entry of the mode inside the Hubble radius, it collapses instantaneously and forms PBH. We define fractional abundance of PBHs as

$$f_{\mathrm{PBH}} = \frac{\rho^{\mathrm{o}}_{\mathrm{PBH}}}{\rho^{\mathrm{o}}_{\mathrm{CDM}}} \tag{6.17}$$

We define mass fraction of PBHs at the formation time as

$$\beta(M_{PBH}) = \frac{\rho_{\mathrm{PBH}}}{\rho_{\mathrm{tot}}} \tag{6.18}$$

During radiation domination, $\beta(M_{PBH})$ behaves as proportional to a ($\rho_{PBH} \simeq a^{-3}$ and $\rho_{tot} \simeq \rho_{rad.} \simeq a^{-4}$). Using the above definition, one can prove that [49] [44] [50]

$$\mathrm{f_{PBH}} = \gamma^{3/2}\, 2^{1/4}\, \beta(M_{\mathrm{PBH}})\, \frac{\Omega^o_M h^2}{\Omega^o_{CDM} h^2} \left(\frac{g_*}{g_{eq.}}\right)^{1/4} \left(\frac{M_{PBH}}{M_{eq.}}\right)^{-1/2} \tag{6.19}$$

where g_* is at the formation time of PBH. $\Omega^0_{\mathrm{M}} h^2$ and $\Omega^0_{\mathrm{CDM}} h^2$ are dimensionless parameters which describe the matter and cold dark matter density at present epoch and values are 0.14 and 0.12 respectively. g_*= 106.75 and $g_{eq.}$= 3.36 are used along with γ = 0.2 (all reference from [44]).

$$f_{PBH} = \left(\frac{\gamma}{0.2}\right)^{3/2} \left(\frac{\beta(M_{PBH})}{1.46 \times 10^{-8}}\right) \left(\frac{g_*}{g_{eq.}}\right)^{-1/4} \left(\frac{M_{PBH}}{M_\odot}\right)^{-1/2} \tag{6.20}$$

Only task is to compute β and this is carried out by employing Press-Schechter formalism [51]. According to Press-Schechter formalism, the density contrast can be characterized using Gaussian distribution and is defined as

$$\mathcal{P}(\delta) = \frac{1}{\sqrt{2\pi\sigma^2}} e^{\left(-\frac{\delta^2}{2\sigma^2}\right)} \tag{6.21}$$

The variance in the Gaussian distribution can be written as an integral over matter power spectrum. We use window function[50] to smoothened the matter power spectrum. Therefore,

$$\sigma^2(R) = \int_0^\infty dlnk\, \mathcal{P}_\delta(k)\, W^2(kR), \tag{6.22}$$

where $W(kR) = e^{-(kR)^2}/2$ and R is scale over which PBH can be formed and it is computed by taking $R = k_{PBH}^{-1}$ (when k_{PBH} is re-entering the Hubble radius). The matter power spectrum and the inflationary power spectrum can be related as [50]

$$\mathcal{P}_\delta(k) = \frac{16}{81}\left(\frac{k}{aH}\right)^4 \mathcal{P}_s(k) \tag{6.23}$$

Hence β, is defined as

$$\beta = \int_{\delta_c}^1 d\delta\, \mathcal{P}(\delta) \simeq \frac{1}{2}\left[1 - \text{erf}\left(\frac{\delta_c}{\sqrt{2\sigma^2}}\right)\right] \tag{6.24}$$

where erf: error function.

So far, we have all the essential elements to investigate the potentials of the interest. In further section, we will present two models: Ultra slow roll (USR) and Punctuated Inflation (PI). We set $M_{\rm Pl} = 1$ and $M_\odot = 1$ for all numerical purposes. For the case when $\beta \ll 1$, then it can be show that

$$\beta \propto \frac{1}{2}\,\text{erfc}\left(\frac{\delta_c}{\sqrt{2}\sigma}\right) \propto \frac{\sigma}{\sqrt{2\pi}\sigma_c} e^{-\delta_c^2/(2\sigma^2)} \tag{6.25}$$

where erfc is complimentary error function. As we can see if we do small change in δ_c or change in relation between R and δ, there would be exponential change in β. Hence, $f_{\rm PBH}$ would change very fastly.

6.5 Models

6.5.1 Ultra Slow Roll Inflation (USR)

A potential of the form is considered [44]

$$V(\phi) = V_o \left[\tanh\left(\frac{\phi}{\sqrt{6}M_{\rm Pl}}\right) + A \sin\left[\frac{\tanh\left(\phi/\sqrt{6}M_{\rm Pl}\right)}{f_\phi}\right]\right]^2 \tag{6.26}$$

where parameters involved have values: V_o = 2 $\times$ 10^{-10} $M_{\rm Pl}^4$, A = 0.130383, f_ϕ = 0.129576.

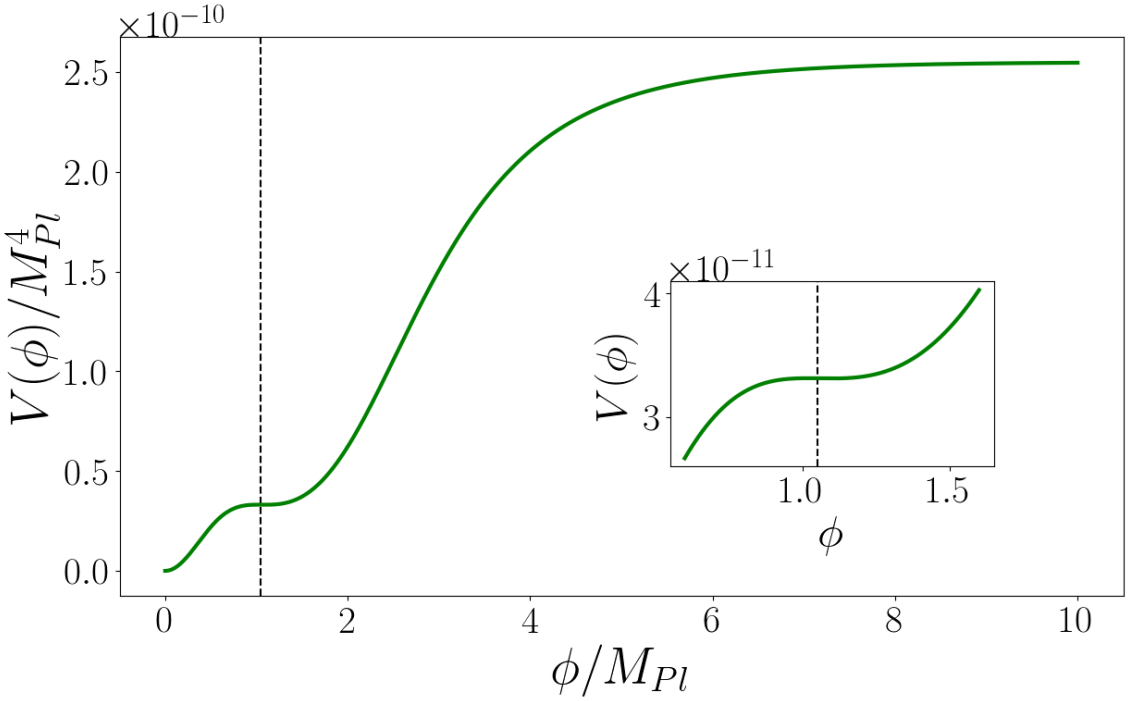

Figure 6.3: USR potential with black dash line as showing the point of inflection at 1.05 $M_{\rm Pl}$. (Plotted using Python).

The point of inflection is at ϕ_o = 1.05 $M_{\rm Pl}$ in fig. (6.3). The initial condition is ϕ_i = 6.1 $M_{\rm Pl}$. The end of the inflation is after 66 e-folds and the pivot scale exits the Hubble radius 56.2 e-folds before the inflation ends. All the values are taken from the ref. [44].

It can be seen that ϵ_2 and ϵ_3 (fig. (6.4a), and (6.4b)) become very large which clearly shows the departure from the slow roll inflation. But ϵ_1 (fig. (6.4c)) becomes very low when it is near by point of inflection. It never touches one during whole process, hence, there is

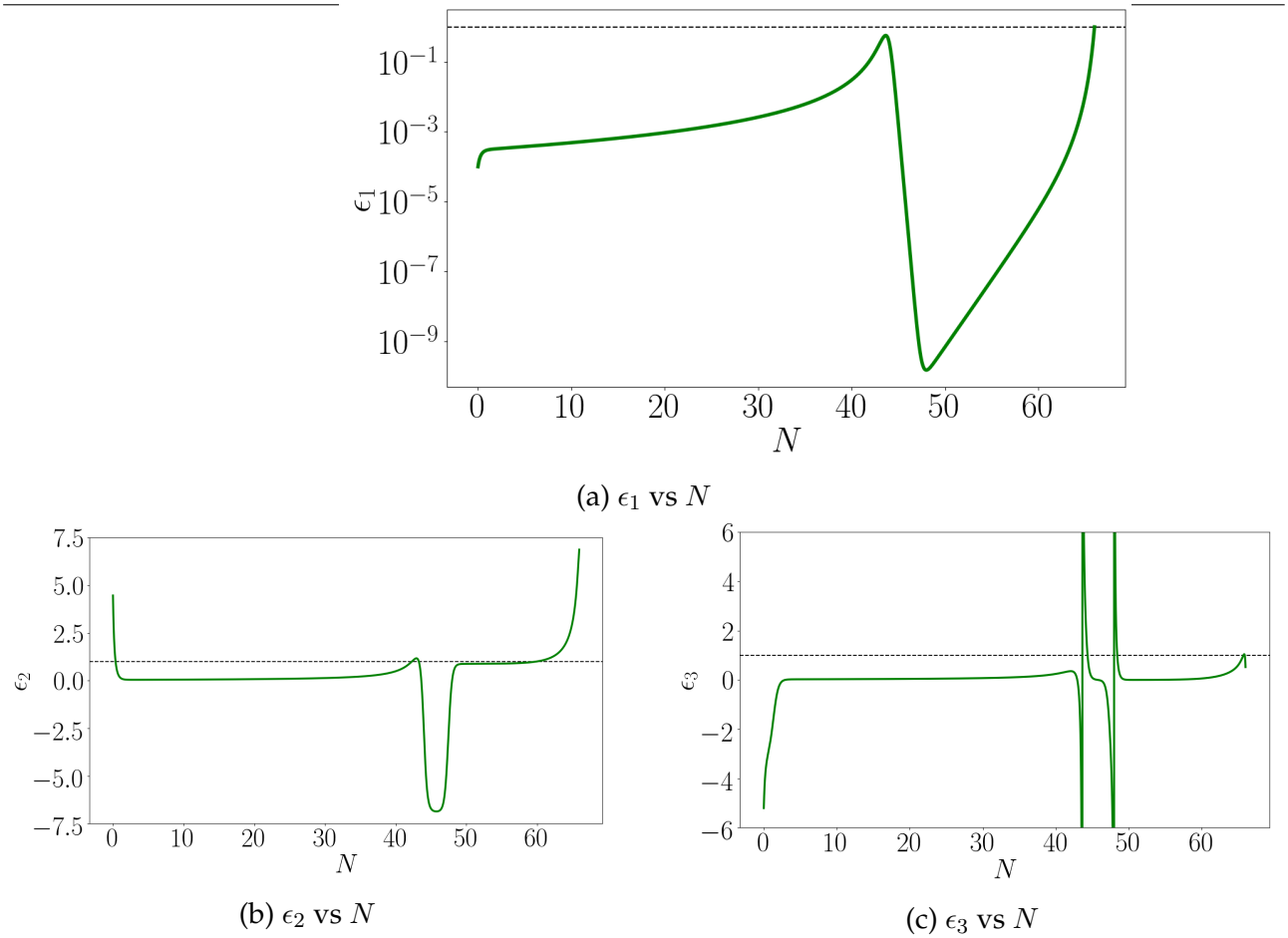

(a) ϵ_1 vs N

(b) ϵ_2 vs N

(c) ϵ_3 vs N

Figure 6.4: Plots of the first, second, and third slow roll parameters for the USR. It is evident that ϵ_2 and ϵ_3 acquire very large values when it reaches inflection point and ϵ_1 does not cross 1 except at the end of the inflation. Hence, there is no interruption of inflation. (Plotted in python by using a self-written code.)

no interruption of inflation. Once ϵ_1 becomes very low, it is in ultra slow roll domain and it rises again to enter the slow roll inflation.

The plot of the scalar power spectrum for the USR model is shown in fig. (6.5). As we can see that it is constrained on the large scales by the CMB data but on small scales it has enhanced. It has the peak value of 1.77×10^{-2} which is sufficient for the production of the PBHs. For finding $f_{\rm PBH}$, we have used three values of δ_c: 1/3, 0.35, and 0.4 (ref. [44]). We can see that in the window $10^{-18}\ M_\odot$ to $10^{-13}\ M_\odot$, there is sufficient contribution of PBH as CDM. For δ_c: 1/3, 0.35, and 0.4, we have maximum value of $f_{\rm PBH}$ as 1.58×10^{-2}, 0.398×10^{-3}, and 2.20×10^{-9}. The maximum contribution to CDM comes from PBH of mass $10^{-15}\ M_\odot$

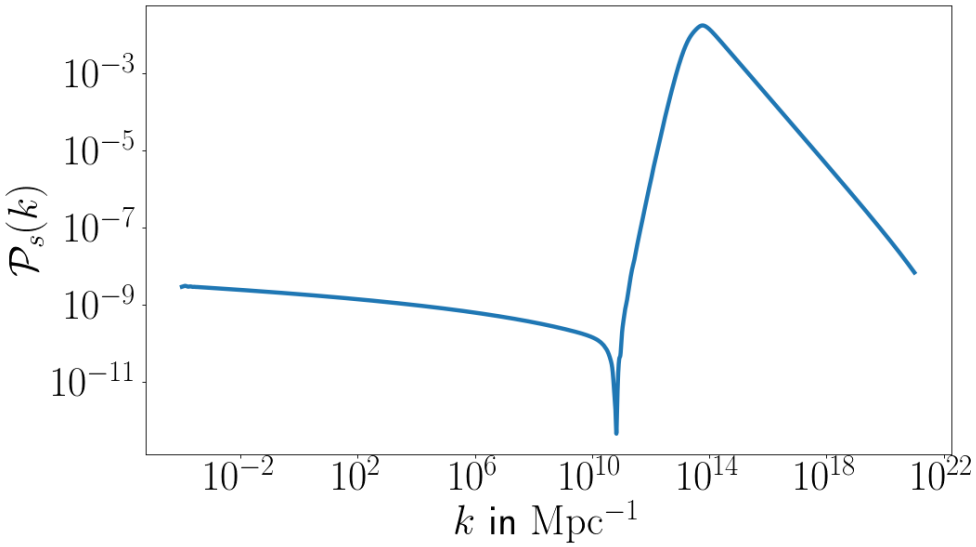

Figure 6.5: Power spectra for the USR model. (Evaluated using a self written code)

6.5.2 Punctuated Inflation (PI)

We choose a potential of the form [44] (fig. 6.7)

$$V(\phi) = V_o \left[c_0 \; + \; c_1 \tanh\left(\frac{\phi}{\sqrt{6}\alpha}\right) \; + \; c_2 \tanh^2\left(\frac{\phi}{\sqrt{6}\alpha}\right) \; + \; c_3 \tanh^3\left(\frac{\phi}{\sqrt{6}\alpha}\right)\right]^2 \qquad (6.27)$$

where parameters involved have values: V_o = 2.1 $\times$ 10^{-10} $M_{\rm Pl}^4$, c_0 = 0.16401, c_1 = 0.3, c_2 = -1.42, c_3 = 2.20313, and α = 1. The inflection point is at ϕ_o = 0.53 $M_{\rm Pl}$. The initial condition is ϕ_i = 7.4 $M_{\rm Pl}$. The end of the inflation is after 68 e-folds and the pivot scale exits the Hubble radius 54.5 e-folds before the end of the inflation. All the values are taken from the ref. [44].

Evidently, ϵ_1 (fig. (6.8a)) crosses unity for a small period before going in ultra slow inflation. This is where inflation interrupts and is the main difference between ultra slow roll potential and punctuated potential. ϵ_2 (fig. (6.8b)) becomes very large when the transition happens from slow roll to ultra slow and ϵ_3 ((6.8c)) blows up when the transition is happening. The plot of the scalar power spectrum is depicted in fig. (6.9) for the PI model. We can observe that on small scales it has enhanced and on large scale it is consistent with CMB observations. It has maximum value 0.01856 at k = 9.68 $\times$ 10^{13} Mpc^{-1} which is of the order of 10^{-2}.

Again same value of δ_c has been used which were used for USR case. Now, the window

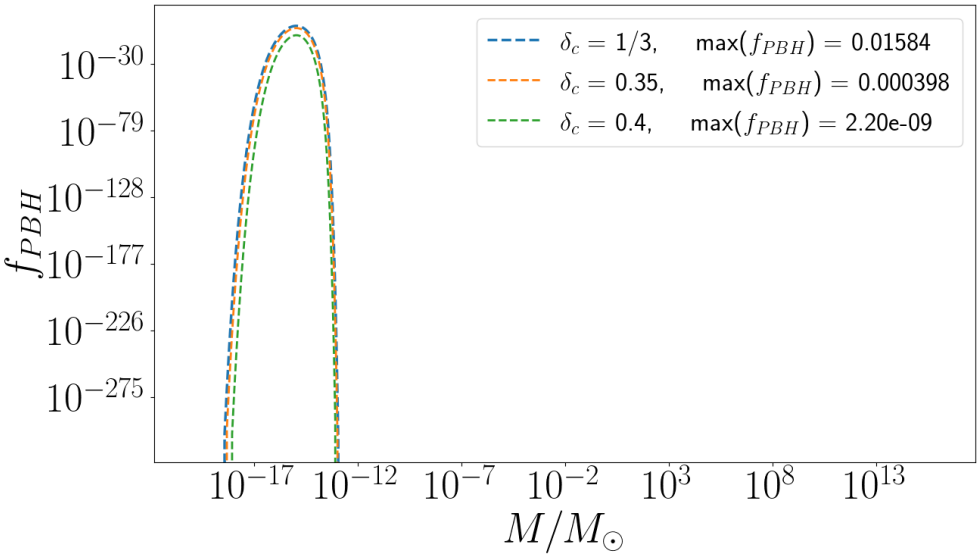

Figure 6.6: f_{PBH} for the USR. (Evaluated using a self written code)

$10^{-18}\ M_\odot$ to $10^{-14}\ M_\odot$ has the contribution of PBH as CDM. The maximum values of f_{PBH} are 3.72×10^{-3}, 7.702×10^{-5}, and 2.26×10^{-10} for δ_c: 1/3, 0.35, and 0.4 respectively. For all three values, maximum contribution to CDM is from PBH of mass $10^{-16}\ M_\odot$

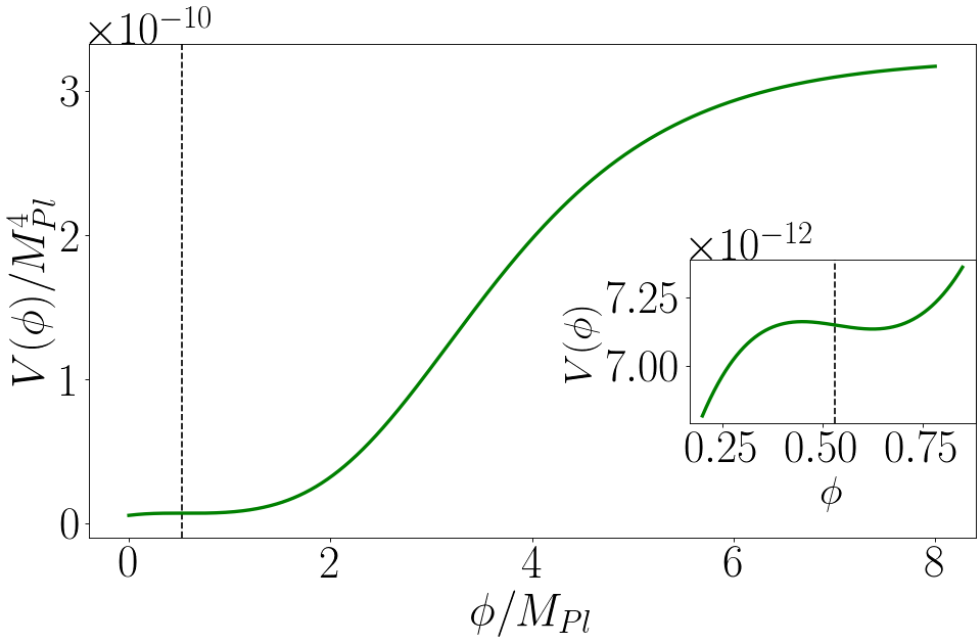

Figure 6.7: PI potential with black dash line as showing the point of inflection at 0.53 $M_{\rm Pl}$ (Plotted using Python).

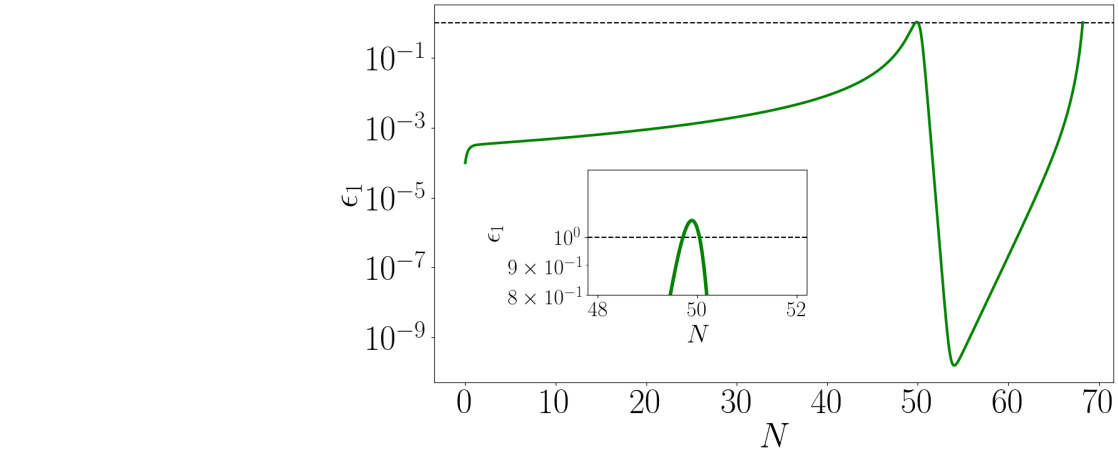

(a) ϵ_1 vs N

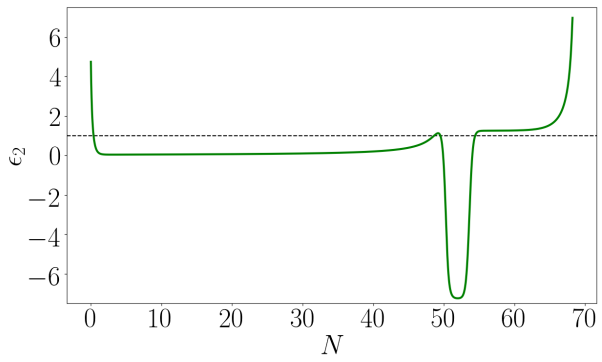

(b) ϵ_2 vs N

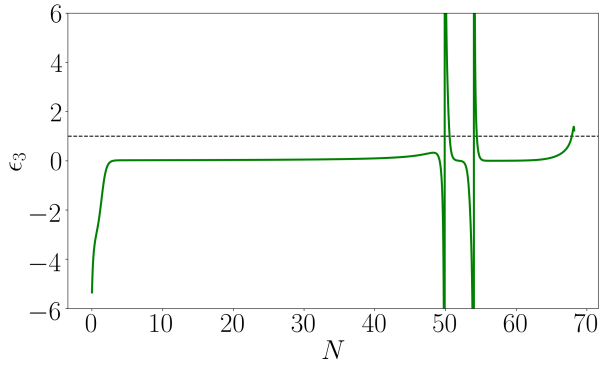

(c) ϵ_3 vs N

Figure 6.8: Plots of the first, second, and third slow roll parameters for the PI. It is evident that ϵ_2 and ϵ_3 acquire very large values when it reaches inflection point and ϵ_1 crosses 1 for a brief period before it hits ultra slow roll domain. Hence, there is interruption of inflation. (Plotted in python by using a self-written code).

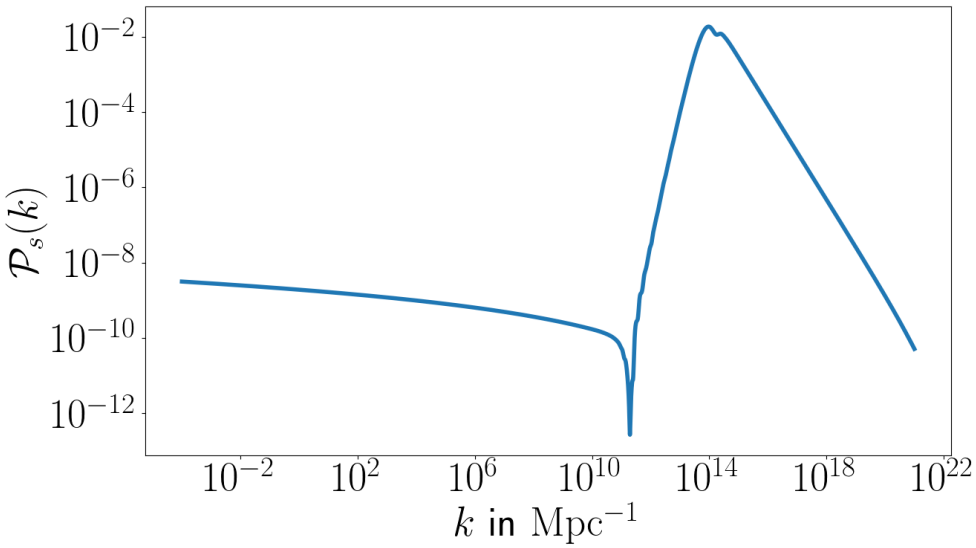

Figure 6.9: Power spectra for the PI model. (Evaluated using a self written code).

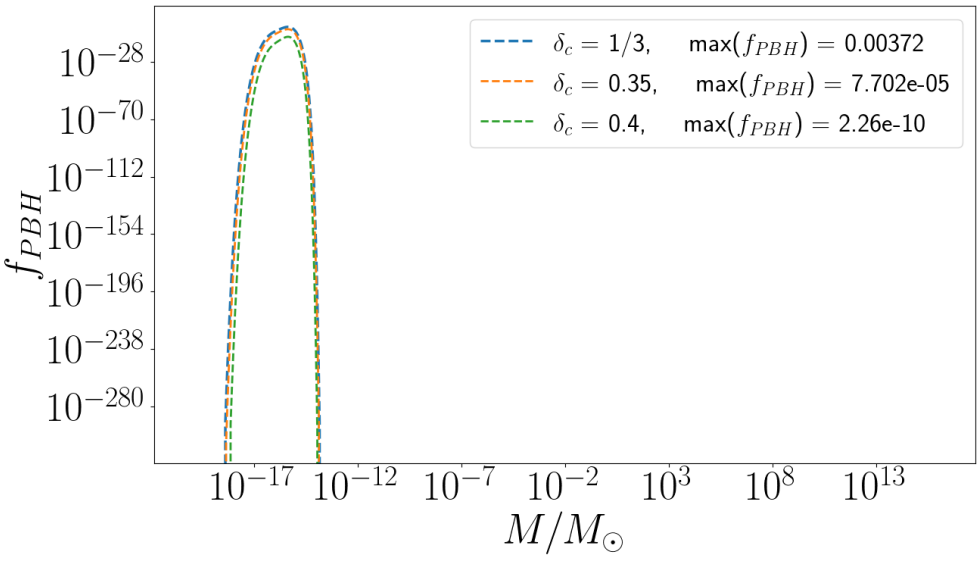

Figure 6.10: f_{PBH} for the PI. (Evaluated using a self written code).

Chapter 7

Observational constraints on f_{PBH}

PBHs have significant impact over cosmology and astrophysics. They leave different observational effects which allow us to constraint their properties. All these constraints are based on electromagnetic signals except gravitational waves. There are two kinds of constraints: Direct and indirect constraints. Direct constraints are based on investigation of observational effects that PBHs could directly trigger by their gravitational properties and are not dependent of the formation mechanism of PBH. They are broadly divided in four categories, namely: Gravitational lensing, Dynamical effects, Accretion, and Large scale structure. Indirect constraints are not connected to the direct observations rather they are based on things which are connected to PBH. These constraints are briefly discussed below and shown in figures (7.1) and (7.2).

- **Hawking radiation (HR)**: Due to HR, PBHs of mass 10^{15} g would have evaporated by now or are evaporating. Moreover, PBHs of small enough mass which are evaporating today should emit strong γ ray and cosmic ray background that could be observed [52].
- **CMB observations**: There are variety of impact due to CMB on f_{PBH}. There are constraints on generation of entropy, spectral distortion of CMB, and CMB anisotropies. PBHs have imprints on CMB. Because of the heat generation, it creates distortion and anisotropies in CMB. The constraint is in the range 10^{13} to 10^{17}g. [53].
- **Lensing effects**: If an compact object passes the line of sight of a star, it is set to produce

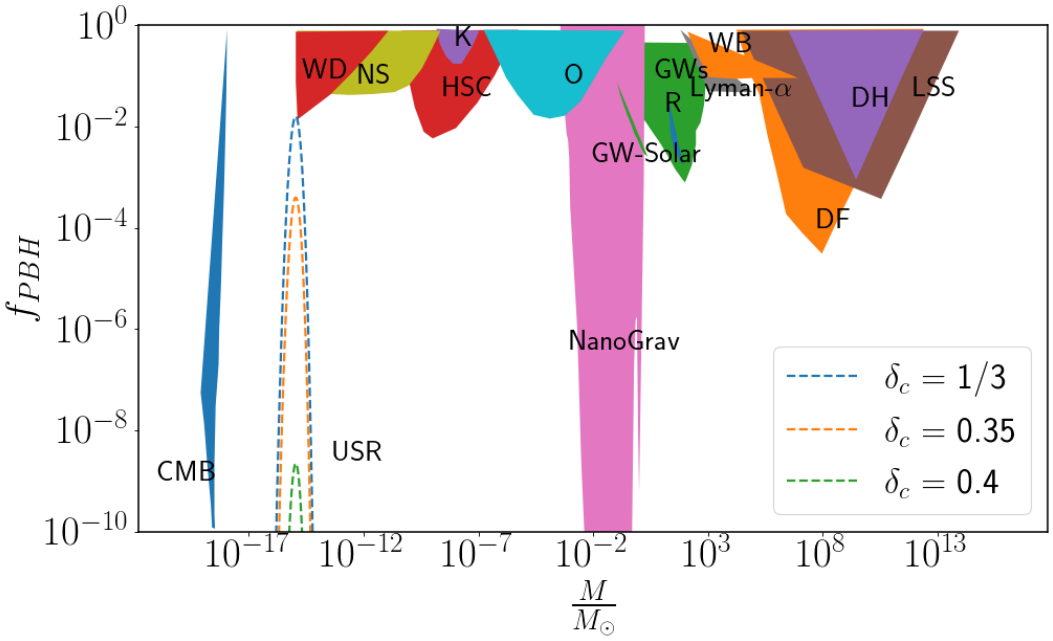

Figure 7.1: Observational constraints on $f_{\rm PBH}$ with USR model prediction. (Evaluated using a self written code based on data available).

micro-lensing effect. Depending on the order of lensing, various events have been observed. For instance, the **Subaru Hyper Supreme Cam (HSC)** [54] observed the M31 and put a constraint on the mass of the PBHs as $10^{-10}\,M_\odot\,to\,10^{-5}\,M_\odot$. Similarly, **KEPLER (K)** [55] mission measured the microlensing effect of our own galaxy and found the limits on PBH mass as $10^{-9}\,M_\odot\,to\,10^{-3}\,M_\odot$. There are constraint due to **OGLE (O)** [13] experiment, which measured the microlensing of both Galactic Bulge and Magellanic Clouds. According to it, PBHs abundance are in the range $10^{-3}\,M_\odot\,to\,10^{-1}\,M_\odot$ for sufficient contribution to $f_{\rm PBH}$.

- **Dynamical constraints**: Various dynamical constraints have been observed where destruction of a variety of astronomical objects take place whenever PBHs pass nearby. Zhilyaev [56] suggested that stars could capture PBHs and they go to center of the star. This produces γ-ray burst (20-300 keV). In case of **White Dwarf (WD)** [57], it can lead to white dwarf explosion. Several authors believe that interaction of PBH and **Neutron Star (NS)** [58] can explain various astronomical phenomena. These put constraints on PBHs mass as $10^{-15}\,M_\odot\,to\,10^{-8}\,M_\odot$. This can also help in explaining the solar-mass

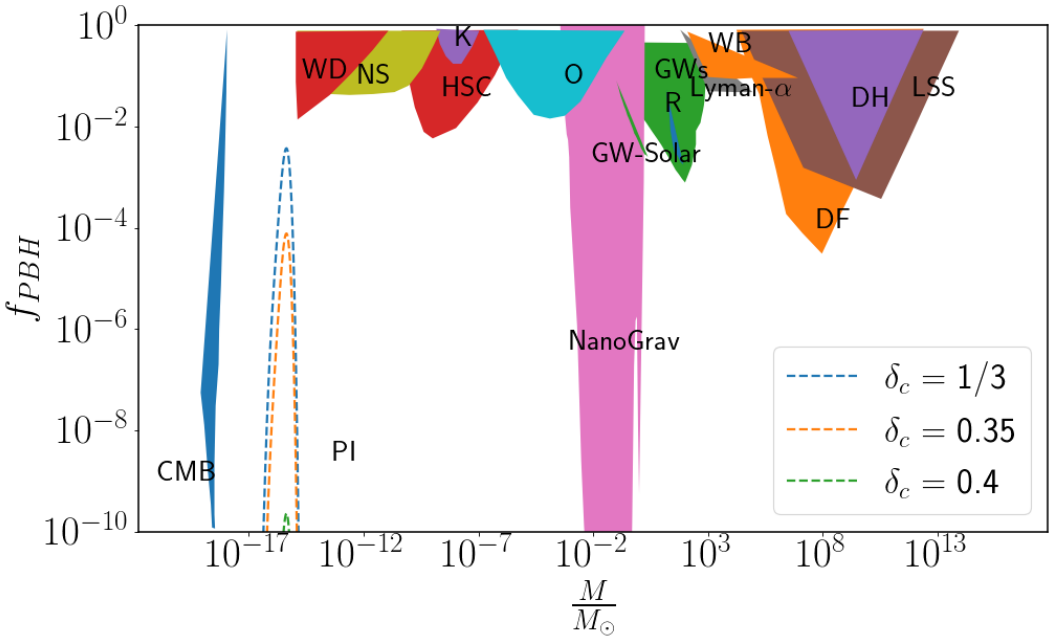

Figure 7.2: Observational constraints on $f_{\rm PBH}$ with PI model prediction. (Evaluated using a self written code based on data available).

PBHs [59].

Binary stars with a large separation are vulnerable to disruption caused by the passage of nearby PBHs. Most of the observations come from the **wide-binaries (WD)**, which constraints the mass of the PBH in the range $10^4\ M_\odot\ to\ 10^7\ M_\odot$ [60].

There are limits in the high mass scale, where the halo objects will overheat the galactic disc. Based on this, PBH mass range lies in $10^6\ M_\odot\ to\ 10^{12}\ M_\odot$ **(DH)**. Whereas another mass range arises because of the **dynamical friction (DF)** of the halo objects which gets dragged in the the galactic nuclei. This leads to PBHs in the range $10^4\ M_\odot\ to\ 10^{12}\ M_\odot$.

- **Large scale structure (LSS)**: Carr and Silk [61] pointed out that even if f_{PBH} is small, PBHs of mass $10^2\ M_\odot$ could generate cosmic structures via the seed or 'Poisson' effect. The constraint is in domain $10^6\ M_\odot\ to\ 10^{12}\ M_\odot$. **Lyman-$\alpha$ forest** [62] observations have been used to obtain an upper limit on mass of the PBH which is $10^4\ M_\odot$ which can contribute significantly to DM.

- **Gravitational wave:** During the first two run of LIGO/Virgo, BHs of the mass 8-51 $M_{\odot}$ [63]were observed. After further analysis, it was found that PBHs could be in the range $10^{1}\, M_{\odot}\, to\, 10^{2}\, M_{\odot}$. There are constraints based on the induced GWs which are calculated based on the 11 years data of Pulsar Timing Array of the North American Nanohertz Observatory for Gravitational waves **(NanoGrav)** [64]. They infer PBHs should be in the mass range 0.0004 - 2 $M_{\odot}$.

Chapter 8

Conclusion

The focus of this chapter will be to summarise the work presented in the report and mention the further work that can be done. Our work is largely based on the production of PBHs using the inflationary scenario.

In the first chapter, we mentioned the history and consequences of the PBHs discovery. We also mentioned about different formation mechanisms of PBH. But we focused particularly on the collapse of the large density fluctuations. We discussed the hot big bang model and the various universe constituents in the second chapter. We also discussed the problem with the hot big bang, i.e., the horizon problem and the flatness problem.

In the third and fourth chapters, we motivated for the need of inflation. We saw how elegantly it resolved both of the problems. Then, we introduced the scalar fields which are necessary for driving the inflation. To have sufficient inflation, we used the slow-roll inflation, and to keep a check on the inflation, we used the slow-roll parameters. We also demonstrated the inflationary attractor, as well as a comparison of analytical and numerical estimates of the inflaton, the first slow roll parameter, and the Hubble parameter. We also introduced perturbation. We classified them as scalar, vector, and tensor. We discussed in detail scalar perturbations and how they can be used to construct a gauge-invariant term R which measures the curvature perturbation. The scalar perturbations were then quantized, and the two-point correlation function: scalar power spectrum was introduced. For the case of slow-roll inflation, we used the Bunch Davies initial condition to estimate the scalar power spectrum at the Hubble crossing.

In the fifth chapter, we discussed three models namely, the quadratic model, small field model, and Starobinsky model. We compared the analytical and the numerical form of the scalar power spectrum. We found that both matches well for all three models. In the sixth chapter, we discussed in detail the PBH formation and its relation with cold dark matter. As slow-roll inflation is insufficient for the PBH formation, we introduced ultra slow-roll inflation and punctuated inflation. The scalar power spectrum was enhanced at small scales while it was consistent at large scales with the Planck CMB data. For the formation of PBH, we used Press Schechter formalism where the collapse of the over-density is dependent on the probability distribution of the density contrast δ. This density contrast has to be greater than a threshold value δ_c. and the probability distribution is Gaussian in nature. We estimated the fraction of cold dark matter due to PBH ($f_{\rm PBH}$). Based on the numerical estimation, we found the mass range and the $f_{\rm PBH}$ in the following table

Model	Mass range	Max. value	$\delta_c = 1/3$	$\delta_c = 0.35$	$\delta_c = 0.4$
USR	$10^{-18}\,M_\odot$ - $10^{-14}\,M_\odot$	$10^{-16}\,M_\odot$	1.5 %	0.03 %	10^{-7} %
PI	$10^{-18}\,M_\odot$ - $10^{-13}\,M_\odot$	$10^{-15}\,M_\odot$	0.3 %	10^{-3} %	10^{-8} %

In the last chapter, we discussed the observational constraints on the $f_{\rm PBH}$ due to various astrophysical and gravitational waves observations such as microlensing effect, gravitational waves, dynamical effects, accretion, large scale structure, and many more. We worked on a single value of a point of inflection and three values of δ_c. One can see the effect of change of inflection point on the scalar power spectrum. This can be utilized to see how it effects the $f_{\rm PBH}$. Further, one can also study the effect of on-Gaussianities.

Appendix A

Proof for relation between k and $M_{\rm PBH}$ for the PBH

For finding the relation between $M_{\rm PBH}$ and k, we will assume that PBHs were formed during radiation domination, therefore, energy and entropy degree of freedom can be assumed to be same, i.e., g_* = g_*^s.
For radiation,

$$\rho \propto g_* T^4. \tag{A.1}$$

According to entropy conservation

$$g_*^2 T^3 a^3 = constant \tag{A.2}$$

Therefore, using above one can prove that

$$\rho \propto g_*^{-1/3} a^{-4}. \tag{A.3}$$

Mass of a PBH is equal to efficiency term (γ) times the horizon mass, i.e., M_{PBH} = $\gamma\, M_H$ = $\gamma/2HG$. Utilising above information, one can find that

$$M_{PBH} = \gamma\sqrt{2}\, M_{eq.} \left(\frac{g_*}{g_{eq.}}\right)^{1/6} \left(\frac{a}{a_{eq.}}\right)^2 \tag{A.4}$$

Using the relation $k_{eq.} = a_{eq.} H_{eq.}$ and $k = aH$ ($k_{eq.}$ and k are modes), we can prove that

$$\frac{k_{eq}}{k} = \sqrt{2}\frac{a}{a_{eq}} \left(\frac{g_{eq}}{g_*}\right)^{-1/6} \tag{A.5}$$

Putting this back in eq. (A.4), one gets

$$M_{PBH} = \frac{\gamma}{\sqrt{2}} M_{eq.} \left(\frac{g_*}{g_{eq.}}\right)^{-1/6} \left(\frac{k}{k_{eq.}}\right)^{-2} \tag{A.6}$$

Fractional abundance of PBHs is

$$f_{\rm PBH} = \frac{\rho^{\rm o}_{\rm PBH}}{\rho^{\rm o}_{\rm CDM}} \tag{A.7}$$

Mass fraction of PBHs at the time of formation is

$$\beta(M_{PBH}) = \frac{\rho_{\rm PBH}}{\rho_{\rm tot}} \tag{A.8}$$

This can simplified to

$$\beta(M_{PBH}) = \frac{\rho_{PBH}}{\rho_{tot}} = \frac{\rho^{\rm o}_{\rm PBH}}{\rho^{\rm o}_{\rm CDM}} \frac{\rho^{\rm o}_{\rm CDM}}{\rho^{\rm o}_{\rm c}} \left(\frac{H_o}{H}\right)^2 \left(\frac{a_o}{a}\right)^2 \tag{A.9}$$

This further simplifies to

$$\beta(M_{PBH}) = \frac{\rho_{PBH}}{\rho_{tot}} = \frac{\rho_{oPBH}}{\rho_{oCDM}} \frac{\rho_{oCDM}}{\rho_{oc}} \left(\frac{H_{eq}}{H}\right)^2 \left(\frac{a_{eq}}{a}\right)^2 \left(\frac{H_o}{H_{eq}}\right)^2 \left(\frac{a_o}{a_{eq}}\right)^2 \tag{A.10}$$

Now using,

$$\left(\frac{H_{eq}}{H}\right)^2 = 2 \left(\frac{g_{eq}}{g_*}\right)^{-1/3} \left(\frac{a}{a_{eq}}\right)^4, \tag{A.11}$$

$$\left(\frac{H_{eq}}{H_o}\right)^2 = \frac{2\,\rho_{om}}{\rho_{oc}} \left(\frac{a_o}{a_{eq}}\right)^3, \tag{A.12}$$

where 2 appears because at the matter-radiation equality $\rho_{tot.\,eq.} = 2\rho_{m.\,eq.} = \rho_{r.\,eq.}$.
Using above ingredients, we obtain

$$f_{\rm PBH} = \gamma^{3/2}\, 2^{1/4}\, \frac{\Omega^o_{\rm M} h^2}{\Omega^o_{\rm CDM} h^2} \left(\frac{g_*}{g_{eq.}}\right)^{1/4} \left(\frac{M_{PBH}}{M_{eq.}}\right)^{-1/2} \tag{A.13}$$

Appendix B

Typical order of $\mathcal{P}_S$ for sufficient production of PBH

As we defined the Fractional abundance of PBHs is

$$f_{PBH} = \frac{\rho^o_{\rm PBH}}{\rho^o_{\rm CDM}} = \int_{\delta_c}^{1} d\delta\, \mathcal{P}(\delta) \tag{B.1}$$

We assumed $\mathcal{P}(\delta)$ to be Gaussian in nature (Press Schechter formalism). The variance of this distribution is defined as

$$\sigma^2(R) = \int_0^{\infty} dlnk\, \mathcal{P}_\delta(k)\, W^2(kR), \tag{B.2}$$

where $W(kR)$ is window function which is Gaussian in nature and R is scale at which PBH is formed, i.e., $R = k^{-1}_{PBH}$. For simplicity assume that $\sigma^2 = \mathcal{P}_s$. Therefore, it can be proved in the limit $1 \ll \delta_c/\sigma$

$$\beta \propto \frac{1}{2}\,\mathrm{erfc}\left(\frac{\delta_c}{\sqrt{2}\sigma}\right) \propto \frac{\sigma}{\sqrt{2\pi}\sigma_c} e^{-\delta_c^2/(2\sigma^2)} \tag{B.3}$$

Now, the variance would be of this Gaussian distribution as an rough estimate be

$$\mathcal{P}_s \sim \sigma^2 \sim \frac{\delta_c^2}{ln(1/\beta)} \sim \frac{0.2}{ln(1/\beta)} \tag{B.4}$$

Therefore, using eq. (6.15), (A.6), and (6.17), for case when $M_{\rm PBH} \sim M_\odot$ and $f_{\rm PBH} \sim 1$, one obtains

$$k \sim 10^7 Mpc^{-1}, \quad a \sim 10^{-8}\, a_{eq} \tag{B.5}$$

and as $\beta \propto a$, so $\beta \sim 10^{-8}$, i.e, one 10 parts per billion of the universe will be needed to form PBH in order to account for all the DM present today [16]. Further,

$$\mathcal{P}_s \sim \frac{0.2}{ln(1/\beta)} \sim \frac{0.2}{ln(10^8)} \sim 10^{-2} \tag{B.6}$$

Bibliography

[1] S. W. Hawking. "Black Holes From Cosmic Strings". In: *Phys. Lett. B* 231 (1989), pp. 237–239. DOI: 10.1016/0370-2693(89)90206-2.

[2] S. W. Hawking, I. G. Moss, and J. M. Stewart. "Bubble Collisions in the Very Early Universe". In: *Phys. Rev. D* 26 (1982), p. 2681. DOI: 10.1103/PhysRevD.26.2681.

[3] M.Yu. Khlopov and A.G. Polnarev. "Primordial black holes as a cosmological test of grand unification". In: *Physics Letters B* 97.3 (1980), pp. 383–387. ISSN: 0370-2693. DOI: https://doi.org/10.1016/0370-2693(80)90624-3. URL: https://www.sciencedirect.com/science/article/pii/0370269380906243.

[4] Teruaki Suyama et al. "Black hole production in tachyonic preheating". In: *Journal of Cosmology and Astroparticle Physics* 2006.04 (2006), pp. 001–001. DOI: 10.1088/1475-7516/2006/04/001. URL: https://doi.org/10.1088%2F1475-7516%2F2006%2F04%2F001.

[5] Teruaki Suyama et al. "Are black holes overproduced during preheating?" In: *Physical Review D* 71.6 (2005). DOI: 10.1103/physrevd.71.063507. URL: https://doi.org/10.1103%2Fphysrevd.71.063507.

[6] Kazunori Kohri, David H Lyth, and Alessandro Melchiorri. "Black hole formation and slow-roll inflation". In: *Journal of Cosmology and Astroparticle Physics* 2008.04 (2008), p. 038. DOI: 10.1088/1475-7516/2008/04/038. URL: https://doi.org/10.1088%2F1475-7516%2F2008%2F04%2F038.

[7] Ya. B. Zel'dovich and I. D. Novikov. "The Hypothesis of Cores Retarded during Expansion and the Hot Cosmological Model". In: 43 (Jan. 1966), p. 758.

[8] Stephen Hawking. "Gravitationally Collapsed Objects of Very Low Mass". In: *Monthly Notices of the Royal Astronomical Society* 152.1 (Apr. 1971), pp. 75–78. ISSN: 0035-8711. DOI: 10.1093/mnras/152.1.75. eprint: https://academic.oup.com/mnras/article-pdf/152/1/75/9360899/mnras152-0075.pdf. URL: https://doi.org/10.1093/mnras/152.1.75.

[9] B. J. Carr. "The primordial black hole mass spectrum." In: 201 (Oct. 1975), pp. 1–19. DOI: 10.1086/153853.

[10] George F. Chapline. "Cosmological effects of primordial black holes". In: *Nature* 253.5489 (1975), pp. 251–252. DOI: 10.1038/253251a0.

[11] C. Alcock et al. "The MACHO Project Large Magellanic Cloud Microlensing Results from the First Two Years and the Nature of the Galactic Dark Halo". In: *The Astrophysical Journal* 486.2 (1997), pp. 697–726. DOI: 10.1086/304535. URL: https://doi.org/10.1086%2F304535.

[12] P. Tisserand et al. "Limits on the Macho content of the Galactic Halo from the EROS-2 Survey of the Magellanic Clouds". In: *Astronomy &amp Astrophysics* 469.2 (2007), pp. 387–404. DOI: 10.1051/0004-6361:20066017. URL: https://doi.org/10.1051%2F0004-6361%3A20066017.

[13] Ł. Wyrzykowski et al. "The OGLE view of microlensing towards the Magellanic Clouds - II. OGLE-II Small Magellanic Cloud data★". In: *Monthly Notices of the Royal Astronomical Society* 407.1 (2010), pp. 189–200. DOI: 10.1111/j.1365-2966.2010.16936.x. URL: https://doi.org/10.1111%2Fj.1365-2966.2010.16936.x.

[14] B. P. Abbott et al. "Tests of General Relativity with GW150914". In: *Phys. Rev. Lett.* 116 (22 2016), p. 221101. DOI: 10.1103/PhysRevLett.116.221101. URL: https://link.aps.org/doi/10.1103/PhysRevLett.116.221101.

[15] Alba Kalaja et al. "From primordial black holes abundance to primordial curvature power spectrum (and back)". In: *Journal of Cosmology and Astroparticle Physics* 2019.10 (2019), pp. 031–031. DOI: 10.1088/1475-7516/2019/10/031. URL: https://doi.org/10.1088%2F1475-7516%2F2019%2F10%2F031.

[16] Christian T. Byrnes, Edmund J. Copeland, and Anne M. Green. "Primordial black holes as a tool for constraining non-Gaussianity". In: *Physical Review D* 86.4 (2012). DOI: 10.1103/physrevd.86.043512. URL: https://doi.org/10.1103%2Fphysrevd.86.043512.

[17] Gabriele Franciolini et al. "Searching for a subpopulation of primordial black holes in LIGO-Virgo gravitational-wave data". In: *Physical Review D* 105.8 (2022). DOI: 10.1103/physrevd.105.083526. URL: https://doi.org/10.1103%2Fphysrevd.105.083526.

[18] Rachel Bean and João Magueijo. "Could supermassive black holes be quintessential primordial black holes?" In: *Phys. Rev. D* 66 (6 2002), p. 063505. DOI: 10.1103/PhysRevD.66.063505. URL: https://link.aps.org/doi/10.1103/PhysRevD.66.063505.

[19] Matthew Collessy. "First results from the 2dF Galaxy Redshift Survey". In: *Philosophical Transactions of the Royal Society of London. Series A: Mathematical, Physical and Engineering Sciences* 357.1750 (1999). Ed. by G. P. Efstathiou et al., pp. 105–116. DOI: 10.1098/rsta.1999.0317. URL: https://doi.org/10.1098%2Frsta.1999.0317.

[20] Donald G. York et al. "The Sloan Digital Sky Survey: Technical Summary". In: *The Astronomical Journal* 120.3 (2000), pp. 1579–1587. DOI: 10.1086/301513. URL: https://doi.org/10.1086%2F301513.

[21] Morag I. Scrimgeour et al. “The WiggleZ Dark Energy Survey: the transition to large-scale cosmic homogeneity”. In: *Monthly Notices of the Royal Astronomical Society* 425.1 (2012), pp. 116–134. DOI: 10.1111/j.1365-2966.2012.21402.x. URL: https://doi.org/10.1111%2Fj.1365-2966.2012.21402.x.

[22] Daniel Baumann. *TASI Lectures on Inflation*. 2012. arXiv: 0907.5424 [hep-th].

[23] Swagat Mishra. “Title: "Some aspects of the Accelerating Universe: from Inflation to Dark Energy".” PhD thesis. July 2021. DOI: 10.13140/RG.2.2.13658.06089.

[24] Andrew R. Liddle. *An introduction to modern cosmology*. 1998.

[25] Antonio Riotto. *Inflation and the Theory of Cosmological Perturbations*. 2002. DOI: 10.48550/ARXIV.HEP-PH/0210162. URL: https://arxiv.org/abs/hep-ph/0210162.

[26] L. Sriramkumar. *An introduction to inflation and cosmological perturbation theory*. 2009. DOI: 10.48550/ARXIV.0904.4584. URL: https://arxiv.org/abs/0904.4584.

[27] William H. Kinney. *TASI Lectures on Inflation*. 2009. arXiv: 0902.1529 [astro-ph.CO].

[28] V. Mukhanov. *Physical Foundations of Cosmology*. Oxford: Cambridge University Press, 2005. ISBN: 978-0-521-56398-7. DOI: 10.1017/CBO9780511790553.

[29] Sagarika Tripathy et al. “Challenges in the choice of the nonconformal coupling function in inflationary magnetogenesis”. In: *Physical Review D* 105.6 (2022). DOI: 10.1103/physrevd.105.063519. URL: https://doi.org/10.1103%2Fphysrevd.105.063519.

[30] Bruce A. Bassett, Shinji Tsujikawa, and David Wands. “Inflation dynamics and reheating”. In: *Reviews of Modern Physics* 78.2 (2006), pp. 537–589. DOI: 10.1103/revmodphys.78.537. URL: https://doi.org/10.1103%2Frevmodphys.78.537.

[31] Scott Dodelson. *Modern Cosmology*. Amsterdam: Academic Press, 2003. ISBN: 978-0-12-219141-1.

[32] L. Sriramkumar and T. R. Seshadri, eds. *Vignettes in Gravitation and Cosmology*. WSP, 2012. ISBN: 978-981-4322-06-5, 978-981-4464-21-5. DOI: 10.1142/7864.

[33] V. F. Mukhanov, H. A. Feldman, and R. H. Brandenberger. “Theory of cosmological perturbations”. In: 215.5-6 (June 1992), pp. 203–333. DOI: 10.1016/0370-1573(92)90044-Z.

[34] D. H. Lyth. “Large-scale energy-density perturbations and inflation”. In: *Phys. Rev. D* 31 (8 1985), pp. 1792–1798. DOI: 10.1103/PhysRevD.31.1792. URL: https://link.aps.org/doi/10.1103/PhysRevD.31.1792.

[35] Jerome Martin. *The Theory of Inflation*. 2018. arXiv: 1807.11075 [astro-ph.CO].

[36] and N. Aghanim et al. “iPlanck/i 2018 results”. In: *Astronomy &amp Astrophysics* 641 (2020), A6. DOI: 10.1051/0004-6361/201833910. URL: https://doi.org/10.1051%2F0004-6361%2F201833910.

[37] S. Shankar Sastry. "Introductory methods of numerical analysis / S.S. Sastry". In: 1984.

[38] Emory F. Bunn, Andrew R. Liddle, and Martin White. "Four-year COBE normalization of inflationary cosmologies". In: *Physical Review D* 54.10 (1996), R5917–R5921. DOI: 10.1103/physrevd.54.r5917. URL: https://doi.org/10.1103%2Fphysrevd.54.r5917.

[39] H. V. Ragavendra, Debika Chowdhury, and L. Sriramkumar. *Suppression of scalar power on large scales and associated bispectra*. 2020. DOI: 10.48550/ARXIV.2003.01099. URL: https://arxiv.org/abs/2003.01099.

[40] Jé rôme Martin and L Sriramkumar. "The scalar bi-spectrum in the Starobinsky model: the equilateral case". In: *Journal of Cosmology and Astroparticle Physics* 2012.01 (2012), pp. 008–008. DOI: 10.1088/1475-7516/2012/01/008. URL: https://doi.org/10.1088%2F1475-7516%2F2012%2F01%2F008.

[41] B. P. Abbott et al. "Observation of Gravitational Waves from a Binary Black Hole Merger". In: *Physical Review Letters* 116.6 (2016). DOI: 10.1103/physrevlett.116.061102. URL: https://doi.org/10.1103%2Fphysrevlett.116.061102.

[42] B. P. Abbott et al. "GW170104: Observation of a 50-Solar-Mass Binary Black Hole Coalescence at Redshift 0.2". In: *Physical Review Letters* 118.22 (2017). DOI: 10.1103/physrevlett.118.221101. URL: https://doi.org/10.1103%2Fphysrevlett.118.221101.

[43] M. P. Hobson, G. P. Efstathiou, and A. N. Lasenby. *General relativity: An introduction for physicists*. 2006.

[44] H. V. Ragavendra et al. "Primordial black holes and secondary gravitational waves from ultraslow roll and punctuated inflation". In: *Physical Review D* 103.8 (2021). DOI: 10.1103/physrevd.103.083510. URL: https://doi.org/10.1103%2Fphysrevd.103.083510.

[45] Christian T. Byrnes and Philippa S. Cole. *Lecture notes on inflation and primordial black holes*. 2021. DOI: 10.48550/ARXIV.2112.05716. URL: https://arxiv.org/abs/2112.05716.

[46] Misao Sasaki et al. "Primordial black holes—perspectives in gravitational wave astronomy". In: *Classical and Quantum Gravity* 35.6 (2018), p. 063001. DOI: 10.1088/1361-6382/aaa7b4. URL: https://doi.org/10.1088%2F1361-6382%2Faaa7b4.

[47] Pablo Villanueva-Domingo, Olga Mena, and Sergio Palomares-Ruiz. "A Brief Review on Primordial Black Holes as Dark Matter". In: *Frontiers in Astronomy and Space Sciences* 8 (2021). DOI: 10.3389/fspas.2021.681084. URL: https://doi.org/10.3389%2Ffspas.2021.681084.

[48] B. J. Carr et al. "New cosmological constraints on primordial black holes". In: *Physical Review D* 81.10 (2010). DOI: 10.1103/physrevd.81.104019. URL: https://doi.org/10.1103%2Fphysrevd.81.104019.

[49] Swagat S. Mishra and Varun Sahni. "Primordial black holes from a tiny bump/dip in the inflaton potential". In: *Journal of Cosmology and Astroparticle Physics* 2020.04 (2020), pp. 007–007. DOI: 10.1088/1475-7516/2020/04/007. URL: https://doi.org/10.1088%2F1475-7516%2F2020%2F04%2F007.

[50] Nilanjandev Bhaumik and Rajeev Kumar Jain. "Primordial black holes dark matter from inflection point models of inflation and the effects of reheating". In: *Journal of Cosmology and Astroparticle Physics* 2020.01 (2020), pp. 037–037. DOI: 10.1088/1475-7516/2020/01/037. URL: https://doi.org/10.1088%2F1475-7516%2F2020%2F01%2F037.

[51] William H. Press and Paul Schechter. "Formation of Galaxies and Clusters of Galaxies by Self-Similar Gravitational Condensation". In: 187 (Feb. 1974), pp. 425–438. DOI: 10.1086/152650.

[52] D. N. Page and S. W. Hawking. "Gamma rays from primordial black holes." In: 206 (May 1976), pp. 1–7. DOI: 10.1086/154350.

[53] Bernard Carr, Florian Kühnel, and Marit Sandstad. "Primordial black holes as dark matter". In: *Physical Review D* 94.8 (2016). DOI: 10.1103/physrevd.94.083504. URL: https://doi.org/10.1103%2Fphysrevd.94.083504.

[54] Hiroko Niikura et al. "Microlensing constraints on primordial black holes with Subaru/HSC Andromeda observations". In: *Nature Astronomy* 3.6 (2019), pp. 524–534. DOI: 10.1038/s41550-019-0723-1. URL: https://doi.org/10.1038%2Fs41550-019-0723-1.

[55] Kim Griest, Agnieszka M. Cieplak, and Matthew J. Lehner. "EXPERIMENTAL LIMITS ON PRIMORDIAL BLACK HOLE DARK MATTER FROM THE FIRST 2 YR OFiKEPLER/iDATA". In: *The Astrophysical Journal* 786.2 (2014), p. 158. DOI: 10.1088/0004-637x/786/2/158. URL: https://doi.org/10.1088%2F0004-637x%2F786%2F2%2F158.

[56] B. E. Zhilyaev. "Gamma-Ray Bursts as Manifestation of Collisions of Primordial Black Holes with Stars". In: (2007). DOI: 10.48550/ARXIV.0706.0930. URL: https://arxiv.org/abs/0706.0930.

[57] Peter W. Graham, Surjeet Rajendran, and Jaime Varela. "Dark matter triggers of supernovae". In: *Physical Review D* 92.6 (2015). DOI: 10.1103/physrevd.92.063007. URL: https://doi.org/10.1103%2Fphysrevd.92.063007.

[58] Fabio Capela, Maxim Pshirkov, and Peter Tinyakov. "Constraints on primordial black holes as dark matter candidates from capture by neutron stars". In: *Physical Review D* 87.12 (2013). DOI: 10.1103/physrevd.87.123524. URL: https://doi.org/10.1103%2Fphysrevd.87.123524.

[59] Volodymyr Takhistov. "Positrons from primordial black hole microquasars and gamma-ray bursts". In: *Physics Letters B* 789 (2019), pp. 538–544. DOI: 10.1016/j.physletb.2018.12.043. URL: https://doi.org/10.1016%2Fj.physletb.2018.12.043.

[60] J. N. Bahcall, P. Hut, and S. Tremaine. "Maximum mass of objects that constitute unseen disk material". In: 290 (Mar. 1985), pp. 15–20. DOI: 10.1086/162953.

[61] Philip Lu et al. "Constraining Primordial Black Holes with Dwarf Galaxy Heating". In: *The Astrophysical Journal Letters* 908.2 (2021), p. L23. DOI: 10.3847/2041-8213/abdcb6. URL: https://doi.org/10.3847%2F2041-8213%2Fabdcb6.

[62] N. Afshordi, P. McDonald, and D. N. Spergel. "Primordial Black Holes as Dark Matter: The Power Spectrum and Evaporation of Early Structures". In: *The Astrophysical Journal* 594.2 (2003), pp. L71–L74. DOI: 10.1086/378763. URL: https://doi.org/10.1086%2F378763.

[63] Simeon Bird et al. "Did LIGO Detect Dark Matter?" In: *Physical Review Letters* 116.20 (2016). DOI: 10.1103/physrevlett.116.201301. URL: https://doi.org/10.1103%2Fphysrevlett.116.201301.

[64] Zu-Cheng Chen, Chen Yuan, and Qing-Guo Huang. "Pulsar Timing Array Constraints on Primordial Black Holes with NANOGrav 11-Year Dataset". In: *Physical Review Letters* 124.25 (2020). DOI: 10.1103/physrevlett.124.251101. URL: https://doi.org/10.1103%2Fphysrevlett.124.251101.